

Model Name: ADCIRC-UnSWAN
Functional Area: Storm Surge and Waves
Model Proponents: Coastal Protection and Restoration Authority
Model Developer(s): ARCADIS

Please note this is a working-draft document currently undergoing review and revision. The final version will be posted in March 2012 along with the final version of the 2012 Coastal Master Plan.

DRAFT

Table of Contents

1. Background	1
a. Purpose of Model	1
b. Model Description and Depiction	1
c. Contribution to Planning Effort.....	3
d. Description of Input Data.....	3
e. Description of Output Data.....	19
f. Statement on the Capabilities and Limitations of the Model.....	24
g. Description of Model Development Process Including Documentation on Testing Conducted (Alpha and Beta tests)	29
2. Technical Quality	29
a. Theory.....	29
b. Description of System being Represented by the Model	33
c. Analytical Requirements.....	33
d. Assumptions.....	34
e. Identification of Formulas Used in the Model and Proof that the Computations are Appropriate and Done Correctly	34
3. System Quality.....	34
a. Description and rationale for selection of supporting Software Tool/Programming Language and Hardware Platform	34
b. Proof that the Programming was Done Correctly	34
c. Availability of Software and Hardware Required by Model.....	34
d. Description of Process Used to Test and Validate Model.....	35
e. Discussion of the Ability to Import Data into Other Software Analysis Tools (interoperability issue).....	39
4. Usability	39
a. Availability of Input Data Necessary to Support the Model	39
b. Formatting of Output in an Understandable Manner	39
c. Usefulness of Results To Support Project Analysis	39
d. Ability to Export Results Into Project Reports	39
e. Training Availability	40
f. Users Documentation Availability and whether it is User Friendly and Complete.....	40
g. Technical Support Availability.....	40
h. Software/Hardware Platform Availability to All or Most Users	40
i. Accessibility of the Model.....	40
j. Transparency of Model and how it Allows for Easy Verification of Calculations and Outputs ...	40
5. Sources of Model Uncertainty.....	40
6. Suggested Model Improvements.....	41

7. Quality Review 42

8. Uncertainty analysis 42

9. References 43

Tables

Table 1 ADCIRC Meshes, Numbers of Nodes, and CPU Hours Used 6

Table 2 LULC Classifications and Associated Manning’s n and Z₀ Values 8

Table 3 PBL Storm Parameters 15

Table 4 Model Initial Conditions Including Sea Level Rise 18

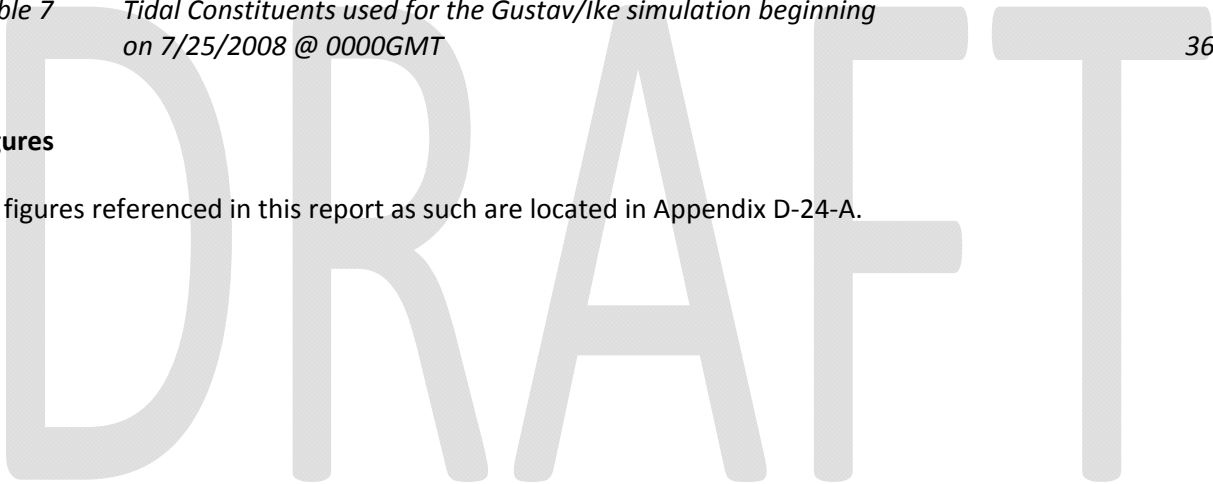
Table 5 Project Attributes 18

Table 6 Data Types passed at Various Point Sets to Risk Assessment Team 24

Table 7 Tidal Constituents used for the Gustav/Ike simulation beginning on 7/25/2008 @ 0000GMT 36

Figures

All figures referenced in this report as such are located in Appendix D-24-A.



1. *Background*

a. **Purpose of Model**

The Advanced CIRCulation (ADCIRC) and Unstructured Simulating WAVes Near-shore (UnSWAN) models are used to compute storm surge and nearshore waves, respectively, throughout the Louisiana coastal area. The models are coupled with wind fields generated by the Planetary Boundary Layer (PBL) model to systematically produce storm surge and wave output that can be understood and analyzed statistically to inform risk and damage assessments. Models are run in a coupled fashion, with varying model inputs to evaluate the change in storm surge and nearshore wave response for current and future conditions, with and without projects.

ADCIRC was selected for this storm surge analysis, as it is a highly vetted and commonly utilized storm surge analysis model. ADCIRC is the standard coastal storm surge model used by the U.S. Army Corps of Engineers (USACE), the National Oceanic and Atmospheric Administration (NOAA) and numerous other organizations. ADCIRC was the model applied in the 2007 coastal Louisiana Flood Insurance Study (FIS) conducted by USACE and the Federal Emergency Management Agency (FEMA), the 2007 Louisiana Coastal Protection and Restoration (LACPR) analysis, the Interagency Performance Evaluation Taskforce (IPET) analysis, and numerous subsequent levee design and risk assessment projects in Louisiana (USACE 2008a, USACE 2008b, USACE 2008c). The methodology applied for this study was established by updating and fine-tuning existing models used previously for the Joint Storm Surge (JSS) Analysis in Southern Louisiana, which consisted of the LACPR project and FEMA FIS. Many model applications and assumptions are based on the findings of JSS study.

ADCIRC has been under continuous development since 1990. The first peer-reviewed publication about ADCIRC was published in 1991. It was developed with funding from the United States Army Corps of Engineers. It is maintained and improved by a users group, in an open source collaborative. This users group is described in www.adcirc.org. The model can simulate a variety of water circulation conditions, including tides, storm surges, tsunamis, relative sea level rise, and other hydrodynamic phenomena. Simulations of flows are used for the design and placement of hydraulic structures, coastal restoration and protection projects, and other scenarios. The model is primarily used by the engineering and scientific community. For planning efforts, the model can provide systematic evaluation of proposed projects, and help planners determine which projects will best satisfy their objectives in the near and long term.

b. **Model Description and Depiction**

The newest generation of ADCIRC model meshes in Louisiana was initially developed by ARCADIS, the University of Notre Dame and USACE in 2005 and 2006 as part of the JSS analysis (USACE 2008a, USACE 2008b, USACE 2008c). The JSS ADCIRC mesh generation is known as SL15, which is short for Southern Louisiana version 15. The state of the art ADCIRC mesh has evolved to SL18 by updating the SL15 mesh as new data become available, such as topographic and bathymetric survey, as well as by increasing resolution as necessary for project analysis (ARCADIS 2008a, ARCADIS 2008b, ARCADIS 2008c, ARCADIS 2008d, ARCADIS 2010, ARCADIS 2011a, ARCADIS 2011b, ARCADIS 2011c). The SL18 mesh includes the most recent and accurate elevation data available throughout Louisiana and notably increased model resolution than the SL15 model. The SL versions of the ADCIRC mesh are highly accurate and robust models that have been thoroughly validated and reviewed by some of leading experts in the field of coastal engineering.

The 2012 Coastal Master Plan model development team was able to leverage the SL mesh development, validation, and application for statistical analysis to create a state of the art ADCIRC-based modeling system specific for the needs of the master plan. This modeling system is subsequently referred to as the *OCPR2012* ADCIRC model. Prior to the development of the *OCPR2012* modeling system, a preliminary study considering the master plan framework was undertaken by OCPRA (now referred to as the Coastal Protection and Restoration Authority or CPRA) to investigate the most cost effective, efficient and accurate means to model storm surge and wave conditions for damage assessment (ARCADIS 2011d). The study considered the application of various numerical models, nesting options, and a scaling analysis to investigate ideal model parameters such as resolution, time step, and parallel computing preferences. The ultimate outcome of the study was the recommendation to utilize a Louisiana coast-wide ADCIRC model, coupled with UnSWAN. The current conditions *OCPR2012* ADCIRC mesh, *OCPR2012_S50*, was developed by retaining critical model features from SL18, such as waterways, levees and other hydraulic controls. The SL18 model features maintained elevation information, as well as model resolution. The *OCPR2012_S50* model strategically derefined the SL18 model away from these features, resulting in a mesh capable of accurately analyzing the breadth of coastal projects in the timeframe necessary to complete the Master Plan analysis.

The ADCIRC model itself is static for this application. The model, as it relates to ADCIRC refers to the actual computational code that is compiled to simulate flow processes. The most recent version of the ADCIRC model, version 49, was applied for this study (Luettich et al. 2010). The ADCIRC hydrodynamic model solves the shallow water equations on unstructured, linear triangular elements. ADCIRC is a physics-based model, using the depth-integrated barotropic equations of mass and momentum conservation subject to the incompressibility, Boussinesq, and hydrostatic pressure approximations. The depth-integrated implementation is used, where the water level and depth-averaged velocity are solved for at each triangle vertex, referred to as nodes.

In this study, ADCIRC has been coupled with the unstructured SWAN (UnSWAN) wave model, which is incorporated into ADCIRC version 49 (Dietrich et al. 2011b). UnSWAN is a spectral wave model which predicts the wave action density spectrum and is applied to estimate nearshore wind-wave growth and transformation to quantify wave parameters, such as wave height, period and direction. Since UnSWAN is a spectral wave model, it does not attempt to resolve processes less than one wavelength, even in areas of very high resolution. Instead, in UnSWAN the waves are described with the two-dimensional wave action density spectrum, even when nonlinear phenomena dominate, such as in the surf zone. It is a third generation wave model to obtain realistic wave estimates of wave parameters for given wind-, bottom-, and current conditions, based on the spectrum evolution in time and space.

ADCIRC was previously coupled with the STeady State Spectral WAVE (STWAVE) nearshore wave model in most previous SL studies, including the JSS. However, the UnSWAN model was selected in this analysis due to its ease of coupling with ADCIRC and recent study findings that UnSWAN displays similar levels of accuracy as structured nearshore wave models such as STWAVE and SWAN (Dietrich et al. 2011a). UnSWAN and STWAVE have been found to produce similar wave outputs and have similar effects on storm surge when hindcasting Hurricanes Ike, Gustav, Rita and Katrina. Dietrich et al. describe this in detail in a recent publication centered on the hindcast of Hurricane Gustav (Dietrich et al. 2011a).

c. Contribution to Planning Effort

Hurricane storm surge modeling using ADCIRC and UnSWAN contributes to the master plan effort by producing storm surge and nearshore wave computations essential to the risk and damage assessment component of the study. The storm surge and wave output is imperative to quantify risk to coastal communities, infrastructure and the ecosystem. Systematically modifying the ADCIRC and UnSWAN model to account for future conditions with and without proposed restoration and protection projects creates storm surge and wave model output unique to each proposed condition. ADCIRC and UnSWAN model output is subsequently used to compute risk levels for future landscape and sea level rise scenarios, as well as the change in risk due to implementation and construction of proposed restoration and protection projects.

Aside from the master plan, ADCIRC modeling is currently being used in a variety of ways for coastal planning. Examples of the types of applications include analysis of the impact of proposed projects on storm surge and nearshore wave propagation; tidal analysis, including tidal prism, velocity, and hydroperiod variance due to restoration projects, levees and gates; impacts of relative sea level rise and subsidence on surge and tides; effects of proposed structures on geomorphology and salinity; and flood protection and coastal restoration feature optimization, design and placement.

d. Description of Input Data

The critical ADCIRC and UnSWAN model inputs for this study are the computational mesh (*OCPR2012*), surface characteristics file (*fort.13*), and system forcing information, such as inflows at the Mississippi and Atchafalaya Rivers, hurricane wind fields, hurricane pressure fields, and tides for validation simulations. ADCIRC and UnSWAN models utilize the same model inputs and thus communicate directly at each node in the computational mesh. All system forcing data in this study are based on or used directly from the JSS study. Model initial conditions and boundary conditions are based on the JSS study, including riverine inflows, regional mean sea level (MSL) approximations and seasonal sea surface adjustments. Additionally, the PBL synthetic wind and pressure fields applied for this study are the identical fields applied as part of the JSS. The exception being, that rather than simulating the 304 synthetic storms outlined in the JSS, this study utilizes a hypothetical storm set of 40 of the 304 synthetic storms to produce storm surge and wave output for use in the Risk Assessment Model (See Appendix D-25 Risk Assessment).

The computational mesh consists of nodes, which are the locations where the ADCIRC model solves the shallow water equations and the UnSWAN model computes wave action density spectrum. Nodes communicate with each other via linear triangular finite elements. The computational modeling process requires that the physical system is accurately described and characterized at the nodal locations. This means that topographic and bathymetric elevations must be accurately represented by the nodes. Figure 1 displays the mesh domain and bathymetric contours of the current conditions version of the mesh, *OCPR2012_s50*. Note that the mesh domain includes the North Atlantic, Caribbean and Gulf of Mexico. The large domain allows the mesh to accurately propagate storm surge through the Caribbean and Gulf of Mexico, onto the continental shelf and overland. Figure 2 shows the mesh domain and elevation contours in the Gulf of Mexico. Louisiana is shown in the northern portion of the domain. Details of the *OCPR2012_s50* elevations along coastal Louisiana for current conditions can be seen in Figures 3 through 5.

Unstructured finite element meshes permit solutions to the shallow water equations that take advantage of highly localized resolution. This study applies coarser element sizes in the open waters

and higher resolution elements near and onshore. *OCPR2012* contains nearly 1.1 million computational nodes and 2.1 million finite elements. Approximately 82 percent of the computational nodes for the *OCPR2012* mesh reside in coastal Louisiana. In the mesh, resolution is focused along the Louisiana coast as a whole and more specifically, in critical areas such as deep draft channels and levees. The elements vary in size from multiple kilometers in the open ocean to resolutions as fine as 15 meters in Louisiana. Varying resolution throughout the mesh domain leads to globally and locally more accurate solutions, while saving on computational expense. Mesh resolution is depicted in Figures 6 through 9. Note that some critical conveyance and impedance areas, such as rivers, dredged channels, levees and highways are highly resolved, while other areas such as the deep waters of the Gulf of Mexico are more coarsely resolved.

Current Conditions Mesh Development and Elevation Assignment

Accurate mapping of the region's elevation data is essential to correctly simulate inland flood propagation. Unique treatment of bathymetry, low lying topography and pronounced vertical features is critical to accurate mapping. Bathymetry and low lying topography influence wind-wave and surge propagation speed, direction, and frictional dissipation, as well as both amplify and attenuate storm surge. Bathymetric areas are typically mapped onto an ADCIRC mesh in a different manner than low lying topography. This is primarily due to the data availability and spatial extent of bathymetric features, particularly narrow and deep waterways. As shown in Figures 6 through 9, narrow bathymetric features require relatively high resolution to adequately capture the conveyance properties of the natural and dredged waterways. Additionally, special attention is given to these waterways when constructing an ADCIRC mesh to assure proper nodal location and elevation assignments to satisfy numerical requirements, such as Courant factor limitations and consideration of the wetting and drying algorithm.

In addition to describing bathymetry and low lying topography, the model must account for pronounced vertical features with small horizontal scales relative to the mesh scale. While pronounced features such as barrier islands, river banks, and salt domes are generally well resolved in meshes, features such as levees, floodwalls, railroads, and raised highways will not be sufficiently resolved with 100-foot mesh resolution. These small-scale features can be significant horizontal obstructions to flow, causing water to rise or be diverted elsewhere. Therefore, these features must be incorporated into the model as sub-mesh scale features or a line of computational nodes along the crown of the feature. Both approaches require strategic positioning both horizontally and vertically. Sub-mesh scale features are included as sub- and super-critical weirs.

As part of the JSS analysis and subsequent applications of the SL generation of ADCIRC meshes, bathymetric and raised features have been strategically positioned and vertically defined. The features are critical components to producing highly accurate simulations using the SL generation of models. Additionally, these features - most notably narrow bathymetric channels - have been stably exercised under various storm surge and wave conditions. A robust model, with a history of accurate results and model stability was required to meet the time constraints of the master plan. Because of this the *OCPR2012* mesh was developed by maintaining the majority of the bathymetric and vertically pronounced features from the SL18 mesh.

SL18 mesh elevation values and mesh resolution are shown in Figures 10 and 11. Note the high resolution of the SL18 mesh, which includes over 6.8 million nodes and 13.5 million elements. All bathymetric features, including those in coastal Louisiana, the nearshore, and offshore were defined using the SL18 mesh nodes and elevations. The Mississippi River and its outlets south of Venice are

the only exception, and were defined using the SL15 mesh. Bathymetry survey for the nearshore and inland waterways was provided by regional bathymetric surveys and dredging surveys, typically from the USACE New Orleans District (MVN) and the National Ocean Service (NOS). Figure 12 shows the inland areas in which the SL mesh generation ADCIRC nodes and elements were directly used as part of the *OCPR2012* mesh. The SL18 mesh elevations were assigned to current conditions (S50) version of the *OCPR2012* mesh. Future conditions S12 (Moderate Future Conditions) and S13 (Less Optimistic Future Conditions) include regional subsidence and accretion, which are accounted for in the mesh, including locations where elevations were established for current conditions using the SL18 mesh. It should also be noted that all topographic and bathymetric values for Texas and Mississippi were interpolated from the SL18 mesh as well.

Similarly, most vertically pronounced features, such as highways, railways, dredge spoil mounds, floodwalls and levees were also maintained from SL18. The exceptions were areas in which new USACE levee and floodwall surveys or new features were implemented. Federal, state, and local roads, levees, and railroads were positioned in the horizontal using the USACE GIS database, Atlas lidar (Louisiana State University 2004), and satellite imagery. The crown elevation for each feature was obtained from federal, state or parish surveys where available. Elsewhere, lidar elevations were extracted automatically by searching a defined region around each node along the pronounced feature. Vertically pronounced features defined using the SL18 model and additional surveys are shown in Figure 13. Green lines represent features that were defined using updated survey or design data which is described in Appendix A - Project Definitions. Yellow lines symbolize areas that utilized SL18 nodal locations and elevations. Black lines employed SL18 feature alignments, but reset elevations using Atlas lidar due to the change in model resolution. Red lines represent features that were repositioned horizontally using lidar and satellite imagery and assigned elevations using lidar.

Though the location of most pronounced vertical features in *OCPR2012* were guided by the SL18 mesh, the treatment of the features is different in many cases. The SL18 mesh uses an internal weir boundary condition for most features while the *OCPR2012* mesh applies a strategically positioned row of nodes along the crown of many features instead of a weir boundary condition. This is the case for all pronounced features south of the Gulf Intracoastal Waterway (GIWW), with the exception of large levees, such as those in Plaquemines Parish. The internal weir boundary conditions were replaced with nodes along feature crowns in order to utilize the shallow water equation approximation of flow when topographic gradients are not too steep relative to horizontal resolution. Using this approach is also beneficial to the UnSWAN model accuracy, which assumes local wave heights are zeroed at weir boundary interfaces. In cases where storm surge elevations are notably higher than the crown of features, a shallow water equation approximation of flow and minimal reduction of wave heights is the most accurate treatment of the physical system. The differenced in weir locations between *OCPR2012* and SL18 can be seen by comparing Figure 3 and Figure 10.

Bathymetric and vertically pronounced features are the primary framework for the *OCPR2012* mesh development. The remainder of coastal Louisiana, as well as portions of Mississippi and Texas, was built outward from the features, nodes and elements that were retained from the SL mesh. Generally, model resolution was reduced substantially from the SL18 model in areas with mild topographic gradients, resulting in areas with resolution as low as 500 to 1,000 meters, as shown in Figures 6 through 9. The parameters for coarsening resolution were defined during the initial phase of this project (ARCADIS 2011d). A key finding was that the SL18 ADCIRC mesh could be successfully

derefining in strategic areas yet still replicate the surge and wave conditions of the SL mesh. The methodologies for derefinement determined during this pilot study were applied to construct the statewide *OCPR2012* mesh. Figure 14 shows a representative hydrograph example from study findings. Model output from mesh version v0.0, which is the full SL16 mesh, was compared to derefined versions (v3.0, v2.0 and v1.0) of a pilot mesh of Barataria Bay. Note that the boundary conditions applied to v3.0, v2.0, and v1.0 were different than v0.0, causing the slightly lower peak surge. Additionally v3.0 was a cutout portion of SL16. The analysis showed that in general, the response values were nearly identical for all three Barataria Bay mesh versions, illustrating that derefinement can be selectively done without a loss in model accuracy. Therefore, where possible, mesh resolution was established in a manner similar to the v1.0 mesh. Table 1 lists the number of mesh nodes and CPU hours required for each mesh.

Table 1 ADCIRC Meshes, Numbers of Nodes, and CPU Hours Used

Mesh	Nodes	CPU Hours
v3.0	922,936	721
v2.0	482,130	413
v1.0	251,087	298

Once nodal locations are determined after derefinement, each node is assigned elevation and surface characteristic information. Nodal elevations not determined using the SL ADCIRC models were set using the U.S. Geological Survey (USGS) digital elevation model (DEM) described in Appendix D-2 – Wetland Morphology Model. The 30-meter resolution DEM was interpolated onto nodes applying mesh scale averaging techniques. The approach to determining area averaged elevations is graphically represented in Figure 15. The red circle in the figure denotes a mesh node. Black lines show mesh elements and blue triangles are the centroids of each element. The maximum extents of the adjacent elemental centroids are determined to establish the area limits used for averaging elevation data for each node. The red dashed box defines this area. All topographic survey data, for instance the DEM, within the red dashed box is averaged and applied to the given node. The size of the area used for mesh scale averaging varies as elemental resolution varies. Note, the current conditions mesh, *OCPR2012_S50*, applied a current conditions DEM for averaging onto nodes. The resulting values are shown in Figures 3 through 5. Future landscapes, such as S12 and S13, applied unique future conditions DEMs. This is discussed in more detail in Appendix D-2 – Wetland Morphology Model.

Mesh scale averaging is applied for two reasons. The first reason is that each ADCIRC node must represent an approximation to the terrain in a region surrounding it. In order to appropriately describe the area, each nodal elevation must incorporate data from the surrounding area rather than from a single data point. The exception to this rule is when vertically pronounced features (such as levees) are included to correctly capture small scale hydraulic conveyances and impedances. The second reason is for model stability purposes. Mesh scale averaging creates a more smooth elevation surface than direct sampling, which in general leads to better model stability.

Horizontal and Vertical Datum

The *OCPR2012* ADCIRC model references water level data to NAVD88. DEM data described in Appendix D-2 – Wetland Morphology Model and levee elevation data described in Appendix A –

Project Definitions are referenced to NAVD88. The SL ADCIRC mesh elevations reference NAVD88, thus all data carried forward from the SL18 and SL15 models utilized the same vertical and horizontal datum as all other data sources. The SL models were constructed using the best known survey data and all survey elevations were adjusted as necessary to maintain a reference to NAVD88. Bathymetric data are typically referenced to Mean Lower Low Water (MLLW). However, during the development of the SL generation of ADCIRC models, NOAA gauges and VDatum resources were utilized to make the appropriate vertical adjustments (USACE 2008b, USACE 2008c).

Current Conditions (Year 0+1 day) Surface Characteristics

In addition to elevation information, ADCIRC requires a description of the terrain roughness over which the wind blows and waves and surge propagate. Surface roughness significantly influences the flow of the overlying fluid, whether it is water or air. In the case of water flowing or waves propagating over a surface, the bottom friction force that is developed is an important resistance mechanism that must be accurately quantified. Manning's n bottom friction resistance formulation is applied to account for surface roughness effects on the water column. This formulation is a widely used standard applied in hydraulic computations. In the case of air flowing over land or water, the wind boundary layer is modified based on an associated surface roughness. Roughness lengths determined by the FEMA hazard loss estimation methodology (HAZUS) program are used to adjust the wind boundary layer (FEMA 2005). A transformation of the wind boundary layer results in a modification to the 10 meters above ground level wind speed and surface drag. Note, the wind boundary layer does not adjust instantaneously to the local roughness but adjusts slowly based on the upwind roughness, as far as 10 kilometers upwind. The third surface roughness that is accounted for is heavily forested canopy. It can be shown that very little wind momentum transfers through heavily forested canopies (Reid and Whitaker 1976). In order to evaluate the reduced air-sea drag force from shielding and canopy, the roughness of the land surface needs to be described.

For this study, land roughness in overland regions is characterized by land cover conditions such as urban, forested, agricultural or marsh as described by datasets such as the USGS land use/land cover (LULC) data discussed in Appendix D-2 – Wetland Morphology Model. For this study, the USGS LULC data, USGS land/water data, Vegetation Model data and NOAA Coastal Change Analysis Program (C-CAP) data are applied. These data sources are described in Appendix D-2 – Wetland Morphology Model, Appendix D-4 – Vegetation Model, and at the NOAA website <http://www.csc.noaa.gov/digitalcoast/data/ccapregional>, respectively. Prior to characterizing land roughness using the land cover data, the four datasets are combined into one continuous 30 meter resolution dataset.

The first step to creating the continuous dataset is to combine USGS LULC data with C-CAP data. Both the USGS LULC and C-CAP data are 30 meter resolution datasets. C-CAP data is incorporated at the outer extents of the USGS data to ensure that the combined LULC data extends beyond the *OCPR2012* mesh domain. The results of the Vegetation Model were added to the other LULC data sets. The Vegetation Model results are provided in 500 meter cells and defined the percentage of each the modeled vegetation types contained in each 500m cell. The vegetation model results were resampled to a 30 meter cell size raster dataset to conform to the cell size of the other data sets. All 30 meter cell averages within a 500 meter cell are applied the same vegetation data as the original 500m cell. The vegetation raster is then combined with the USGS LULC and C-CAP dataset by overwriting USGS and C-CAP cells with vegetation data where it existed. Lastly, the water cells from the 30 meter resolution USGS land/water files were given the highest priority. Thus, all

locations where water existed in the land/water file were set to a water class throughout the combined dataset. Note that for cells incorporating information from the vegetation model, the percentage of vegetation types is scaled appropriately to account for water cells that fall within the 500 meter vegetation cell. This step is necessary to ensure that the percentage of water in a 30 meter resampled cell is not accounted for twice. The result is a continuous, derived data set that covers the extent of the computational domain. The spatial extents of these datasets for current conditions are shown in Figure 16.

The continuous land cover dataset is then applied to the *OCPR2012* mesh using grid scale averaging techniques in the same manner as topography is applied from the DEM. In order to apply land cover data, each land cover or vegetation type is assigned a hydraulic bottom roughness and roughness length to adjust the wind boundary layer. The Manning's n associated with these land classifications was selected or interpolated/extrapolated from standard hydraulic literature (Chow 1959, Henderson 1966, Arcement and Schneider 1989, Barnes 1967). The roughness lengths or more specifically "nominal" roughness lengths Z_0 used to adjust the wind boundary layer are defined by the FEMA HAZUS program (FEMA 2005). Because the FEMA HAZUS definitions were specifically defined for the National Land Cover Data (NLCD), an interpreted version of the NLCD values was used in order to define the roughness lengths. Additionally, the designation of Manning's n and Z_0 values for each class were guided by the selection in previous studies, most notably the Hurricane Gustav validation by Dietrich et al. and the JSS analysis (Dietrich et al. 2011a, USACE 2008a, USACE 2008b, USACE 2008c). The final classifications associated with Manning's n and Z_0 that were selected are given in Table 2.

Table 2 LULC Classifications and Associated Manning's n and Z_0 Values

ID No.	Source	Class Name	Manning's n	Z_0
1	USGS LU/LC	High Intensity Developed	0.120	0.500
2	USGS LU/LC	Medium Intensity Developed	0.120	0.390
3	USGS LU/LC	Low Intensity Developed	0.120	0.500
4	USGS LU/LC	Developed Open Space	0.035	0.330
5	USGS LU/LC	Cultivated	0.050	0.060
6	USGS LU/LC	Pasture/Hay	0.055	0.060
7	USGS LU/LC	Grassland	0.035	0.040
8	Vegetation Model	Bare Land	0.030	0.090
9	USGS LU/LC	Upland Evergreen Forest - Longleaf/Slash Pine Group	0.180	0.720
10	USGS LU/LC	Upland Evergreen Forest - Loblolly/Shortleaf Pine Group	0.180	0.720
11	USGS LU/LC	Upland Mixed Forest - Southern yellow pine/mixed hardwoods	0.170	0.710
12	USGS LU/LC	Upland Deciduous Forest - Mixed upland hardwoods	0.160	0.650
13	USGS LU/LC	PFW-Southern yellow pine/mixed hardwood group	0.150	0.550
14	USGS LU/LC	Palustrine Forested Wetland - Bottomland Ridges - Sweetgum/yellow popl	0.150	0.550
15	USGS LU/LC	Palustrine Forested Wetland - Bottomland - Sugarberry/elm/green ash	0.150	0.550

Table 2 LULC Classifications and Associated Manning's n and Z_0 Values

ID No.	Source	Class Name	Manning's n	Z_0
16	USGS LU/LC	Palustrine Forested Wetland - Bottomland - Nuttall oak/sweetgum/willow	0.150	0.550
17	USGS LU/LC	Palustrine Forested Wetland - Bottomland Ridges - Cottonwood/willow/Sy	0.150	0.550
18	USGS LU/LC	Palustrine Forested Wetland - Bottomland - Overcup oak/water hickory	0.150	0.550
19	USGS LU/LC	Palustrine Forested Wetland - Swamp - Sweetbay/tupelo/red maple	0.075	0.330
20	Vegetation Model	Palustrine Forested Wetland - Swamp - Cypress/tupelo	0.120	0.330
21	USGS LU/LC	Palustrine Forested Wetland - Swamp - Red maple lowland	0.075	0.330
22	Vegetation Model	Palustrine Scrub/Shrub Wetland	0.075	0.150
23	Vegetation Model	Scrub/Shrub Wetland - Wax Myrtle	0.080	0.150
24	Vegetation Model	Estuarine Scrub/Shrub Wetland - Black Mangrove	0.070	0.150
25	Vegetation Model	Palustrine herbaceous wetlands - delta splay	0.060	0.100
26	Vegetation Model	Palustrine herbaceous wetlands - cutgrass	0.070	0.150
27	Vegetation Model	Palustrine herbaceous wetlands – maiden cane	0.065	0.125
28	Vegetation Model	Palustrine herbaceous wetlands - thin mat	0.060	0.100
29	Vegetation Model	Palustrine herbaceous wetlands - cattail	0.070	0.150
30	Vegetation Model	Palustrine herbaceous wetlands – sawgrass	0.070	0.150
31	Vegetation Model	Intermediate herbaceous marsh – bull tongue	0.055	0.125
32	Vegetation Model	Intermediate herbaceous marsh – Roseau cane	0.070	0.150
33	Vegetation Model	Intermediate herbaceous marsh - bullwhip	0.060	0.150
34	Vegetation Model	Brackish herbaceous marsh - wiregrass	0.063	0.100
35	Vegetation Model	Brackish herbaceous marsh - paspalum	0.055	0.125
36	Vegetation Model	Brackish herbaceous marsh-wiregrass/saltgrass/oystergrass	0.055	0.100
37	Vegetation Model	Salt herbaceous marsh - needle grass	0.035	0.100
38	Vegetation	Salt herbaceous marsh - saltgrass	0.035	0.100

Table 2 LULC Classifications and Associated Manning's n and Z_0 Values

ID No.	Source	Class Name	Manning's n	Z_0
	Model			
39	Vegetation Model	Salt herbaceous marsh - oystergrass	0.035	0.100
40	Land/Water	Water	0.025	0.001
41	USGS LU/LC	Sub-aquatic vegetation	0.030	0.001
102	C-CAP	High Intensity Developed	0.120	0.500
103	C-CAP	Medium Intensity Developed	0.120	0.390
104	C-CAP	Low Intensity Developed	0.120	0.500
105	C-CAP	Developed Open Space	0.035	0.330
106	C-CAP	Cultivated Land	0.100	0.060
107	C-CAP	Pasture/Hay	0.055	0.060
108	C-CAP	Grassland	0.035	0.040
109	C-CAP	Deciduous Forest	0.160	0.650
110	C-CAP	Evergreen Forest	0.180	0.720
111	C-CAP	Mixed Forest	0.170	0.710
112	C-CAP	Scrub/Shrub	0.080	0.120
113	C-CAP	Palustrine Forested Wetland	0.150	0.550
114	C-CAP	Palustrine Scrub/Shrub Wetland	0.075	0.110
115	C-CAP	Palustrine Emergent Wetland	0.070	0.110
116	C-CAP	Estuarine Forested Wetland	0.150	0.550
117	C-CAP	Estuarine Scrub/Shrub Wetland	0.070	0.120
118	C-CAP	Estuarine Emergent Wetland	0.060	0.110
119	C-CAP	Unconsolidated Shore	0.030	0.090
120	C-CAP	Bare Land	0.030	0.090
121	C-CAP	Open Water	0.025	0.001
122	C-CAP	Palustrine Aquatic Bed	0.035	0.040
123	C-CAP	Estuarine Aquatic Bed	0.030	0.040

Current condition, OCP2012_s50, Manning's n values are shown in Figures 17 through 20. Note the increased frictional values in forested and developed areas relative to marshes and open water. Throughout the domain, the standard quadratic parameterization of bottom stress is applied. In order to model the spatially variable frictional losses, a Manning's n formulation is applied in order to compute the bottom friction coefficient (C_f),

$$C_f = \left[\frac{g n^2}{H^{1/3}} \right] \quad (1)$$

where g is acceleration due to gravity, H is the total water column height and n is the Manning's coefficient. Bottom friction coefficient values are computed for a specific node and water column height. Previous studies that applied the ADCIRC version 46 also employed a lower limit for C_f of 0.003. This study utilized ADCIRC version 49, without a lower limit to the bottom friction coefficient.

Figures 21 through 24 display directional wind reduction coefficients (Z_0) values for southerly winds, while Figures 25 through 28 display values for northerly winds. Again, note the increased wind reduction in forested and developed areas, relative to marshes and open water as well as the wind boundary layer lag for winds coming off and onto land in nearshore regions. Wind boundary layer re-adjustments depend upon roughness conditions upwind of the location because the wind boundary layer does not adjust to a new roughness instantaneously. Therefore, Z_0 upwind wind reduction factors are computed for 12 directions about the compass by examining all roughness coefficients up to six miles upwind, two of which are shown in Figures 21 through 28. Then, the directional roughness used at each computational point within the mesh is based upon the existing wind direction. This upwind effect is particularly important in the nearshore region where winds are traveling either off or onshore and transitioning to or from open marine conditions. The directional roughness/wind reduction factors were computed with a weighted average of the roughness lengths for all pixels upwind of the computational mesh node in the land classification raster image. Twelve upwind directions are chosen (every 30 degrees about the compass) so that each computational node chooses the closest of the 12 directional roughness/reduction factor directions to the current wind direction. Our approach has been to compute an arithmetic average using land cover data within a control volume around each ADCIRC node. That way, the roughness field is defined at the appropriate grid scale, meaning a finer discretization produces a more detailed characterization of the roughness while a coarser discretization captures a larger-scale average. The weighted land roughness Z_0 within six miles upwind of the computational node are added together to get the weighted upwind land roughness coefficient:

$$z_{0, \text{land-directional}} = \frac{\sum_{i=0}^n w(i) z_{0, \text{land}}(i)}{\sum_{i=0}^n w(i)} \quad (2)$$

where the normalization parameter is computed by an inverse distance weighted average according to:

$$w(i) = \frac{1}{\sqrt{2\pi}\sigma} e^{-\left(\frac{d(i)^2}{2\sigma^2}\right)} \quad (3)$$

The distance from the computational mesh node and the pixel $d(i)$ is limited to six miles in each of the 12 directions. The weighting parameter σ determines the importance of the closest pixels and is set to four miles.

Each of the 12 equal 30-degree slices are split into five linear rays, each ray starting at the coordinates of the node and extending radially six miles distant. The computations incorporate every land cover pixel along the ray and use these values in the weighted averaging formula given. Finally, the five ray averages are averaged to get an average Z_0 value for each 30-degree slice at each ADCIRC node. The resulting upwind effect is particularly important in the nearshore region and results in reduced winds offshore when winds come from land and results in sustained marine winds overland when winds come off the water. Standard non-directional land masking procedures would incorrectly produce full marine winds in the near-offshore zone when winds come from land and result in reduced marine winds in the near-overland zone when winds come off the water. It is in these nearshore and low-lying overland regions experiencing either drawdown or flooding that accurate winds are critical because the wind stress term in the shallow water equations is inversely proportional to total water column height and thus the sensitivity to these winds is the greatest.

An additional consideration when establishing model surface characteristics is that directional wind boundary layer adjustments do not characterize how the wind penetrates the physical roughness elements, such as heavily forested canopies. There are large-scale features that shelter the water surface from the wind stress and they are in effect two-layered systems. Because these large roughness elements are exposed to the hurricane winds, shear stress at the water column surface is much smaller. It can be demonstrated that very little momentum transfer occurs from the wind field to the water column in heavily canopied areas (Reid and Whitaker 1976). Thus canopied areas can be identified with regions where the land cover data defines forested areas. In canopied areas, no wind stress is applied to model the limited impact wind shear stress has on the water column in these areas. The resulting canopied areas in the *OCPR2012* model are shown in Figures 29 through 31. It should be noted that canopied areas do not change between current and future model scenarios, as forested land cover types are supplied in the USGS LU/LC dataset, which remains constant between current and future landscapes.

Two additional surface parameters that are included in the model setup are lateral eddy viscosity and the numerical parameter τ_0 . Both parameters were mapped from the SL18 model (ARCADIS 2011d) and similar to the canopy parameter, both are static for current and future conditions. An eddy viscosity type closure model is applied to account for momentum diffusion and dispersion due to unresolved lateral scales of motion, as well as the effects of depth averaging. A simple version of the standard isotropic and homogeneous eddy viscosity model implemented by Kolar and Gray (1990) is used, where the depth averaged horizontal eddy viscosity coefficient is constant. For this study, a value of $2 \text{ m}^2 \text{ s}^{-1}$ is applied to bathymetry and low lying, highly resolved topographic regions and a value of $20 \text{ m}^2 \text{ s}^{-1}$ is applied elsewhere. Figures 32 through 34 show the eddy viscosity values in the *OCPR2012* model. The τ_0 parameter, discussed in more detail in Section 2a, controls the dispersion properties of the solution and optimizes phase propagation properties. Figure 35 displays τ_0 values through the Gulf of Mexico in the *OCPR2012* model.

Model Initial Conditions

Because the NAVD88 datum is a geodetic equipotential surface, the ADCIRC model requires that initial water levels be raised in the model to account for the fact that average Local MSL (LMSL) lies above zero NAVD88 for most of the year. The JSS analysis examined eleven NOAA benchmarks in Southeastern Louisiana and showed that on average LMSL is 0.44 foot above NAVD88, with a standard deviation equal to 0.15 foot (USACE 2008b, Garster et al. 2007). Additionally, model initial conditions account for the annual fluctuation in sea level due to thermal expansion of the upper layers of the Gulf of Mexico and by other effects including coastal currents, riverine runoff, salinity variations, seasonally prevailing winds and atmospheric pressure. This annual sea surface fluctuation, largely due to the steric effect, clearly presents itself in water level time history records as well as long-term harmonic tidal analyses. The LACPR study estimated sea surface differential based on NOAA long-term sea level stations in the region (NOAA 2007). For the hypothetical storm set, LACPR assumed a maximum end of summer increase of 0.76 foot (USACE 2008a, ARCADIS 2008d).

Initial water levels in all regions of the *OCPR2012* ADCIRC model are therefore raised at the start of the computation with the combined yearly averaged regional difference between LMSL and NAVD88 in addition to the seasonal increase in water level. For the hypothetical storm set, a NAVD88 elevation of 1.20 feet (0.44 foot + 0.76 foot) was applied. Validation simulations apply a different

seasonal adjustment based on the landfall date and thus apply an initial condition specific to each storm. This is discussed on more detail in Section 3d.

Model Time Step

ADCIRC and UnSWAN step through time together on the same unstructured mesh. ADCIRC applies a one second time step for *OCPR2012*, as ADCIRC is limited by wetting and drying criteria as well as other numerical parameters. UnSWAN can take much larger time steps than ADCIRC and during the study, a 1200 second time step was used for UnSWAN. This means that ADCIRC is run for 1200 seconds, at which point information about water levels, currents winds, and wind speeds are passed to the UnSWAN model. UnSWAN was then run at a 1200 second time step and passed information back to ADCIRC, primarily radiation stress gradients. ADCIRC has access to both the radiation stress gradients from the beginning and end of the UnSWAN time step. ADCIRC then extrapolates these gradients forward in time for use in the next 1200 seconds until UnSWAN is run again. UnSWAN uses averaged water levels, currents and wind speeds during its time step.

Model Boundary Conditions

It is critical that boundary location and boundary condition specification do not degrade the model response or introduce non-physical artifacts. The *OCPR2012* mesh employs similar logic as the SL18 mesh to determine boundary placement and specification. The mesh boundaries include an open boundary in the North Atlantic at 60 degrees West, major river flows, no flow boundaries at some mesh perimeter locations such as the Gulf of Mexico and North Atlantic, and internal and external weir boundary conditions.

The open boundary in the North Atlantic is primarily used as a tidal boundary. While tidal conditions are not considered during the application of synthetic storms, tides are important to properly hindcast events such as Hurricane Gustav and Hurricane Ike. These hindcasts are described in Section 3d. For tidal simulations, the open ocean boundary is forced with the K1, O1, M2, S2, and N2 tidal constituents, interpolating tidal amplitude and phase from Le Provost's global tidal model based upon satellite altimetry (Le Provost et al. 1998) onto the open ocean boundary nodes. Second, tidal potential forcing that incorporates an appropriate effective earth elasticity factor for each constituent was applied on the interior of the domain for these same constituents (Westerink et al. 1994, Mukai et al. 2002). The nodal factor and equilibrium argument for boundary and interior domain forcing tidal constituents were determined based on the starting time of the simulation (Luettich and Westerink 2004).

Many structures, such as levees and roadways, are implemented as sub-grid scale parameterized weirs within the domain. These weir locations are shown as brown lines in Figures 3 through 5. ADCIRC defines these barrier boundaries by a pair of computational nodes with a specified crown elevation (Westerink et al. 2001). Once the water level elevation exceeds the crown elevation, the flow across the structure is computed according to basic weir formulae. This is accomplished by examining each node in the defined pair for their respective water surface elevations and computing flow according to the difference in water elevation. The resulting flux is specified as a normal flow from the node with the higher water level to the node with the lower water level for each node pair.

Weir boundary conditions also are implemented for external barrier boundaries, which permit surge that overtops levee structures at the edge of the domain to transmit flow out of the computational area. External weir boundaries were placed in many locations along the inland boundary of the

OCPR2012 mesh, including locations without notable structures or pronounced features. Use of external weir boundary conditions reduced the overall domain size and thus computational cost of the model. Applying external weir boundaries allows flows to leave the system, rather than unnaturally building against a traditional no flow boundary type. The SL18 domain is extended to the 12 meter contour. Conversely, the *OCPR2012* domain extents are defined by the extents of output locations required for the damage and risk assessment portion of the study. Beyond the output locations, external weir boundaries are applied. Comparing Figure 3 and Figure 10 shows the change in model limits between *OCPR2012* and SL18, while comparing Figure 7 and Figure 11 gives a general idea on the computational cost savings of reducing the mesh size and implementing external weir boundaries. Figures 36 through 39 display the outpoint point locations, which are further discussed in Section 1e.

Flows from major rivers, the Mississippi and Atchafalaya, are explicitly incorporated into the model and thus their effect on LMSL in the respective deltas is accounted for explicitly. Not all river flows are included in the model, which can result in small, localized increases in open water LMSL. However, river flows were only absent in the model when their effects are assumed to have an insignificant effect on the resulting water levels.

Mississippi and Atchafalaya River flow rates and river stages were applied based on assumptions from the JSS analysis, using average flow rates from May through September. The Mississippi and Atchafalaya rivers were forced with steady flows of 167,000 cfs and 70,000 cfs, respectively, for synthetic storm simulations. Historical hindcasts are simulated with discharge values averaged over the time of the storm available from stream gauge data from the hurricane event. The Mississippi River boundary condition is placed near Convent, LA. The Atchafalaya River boundary condition is placed immediately south of the Spice Island Chute/Little Devil Cut intersection with the main channel of the river. At river boundaries, a simple elevation or flux boundary condition would reflect tides and surge waves that are propagating upriver back into the domain. In order to prevent this non-physical reflection from occurring, a wave radiation boundary condition was developed that specifies flux into the domain while allowing surface waves to propagate out (Luettich and Westerink 2003). The radiation condition is based on the relationship between the normal flow and elevation at the boundary. River inflow to the Mississippi River and to the Atchafalaya River is specified as a flux per unit width as defined by the wave radiation boundary condition. A 2-day spin-up period with a 0.5-day hyperbolic ramping function is applied to the river boundary forcing prior to any additional model forcing. This allows for a dynamic steady state in the rivers to be established prior to interaction with any other forcing terms to properly define pre-tide and pre-storm river stage on the boundaries.

Wind and Pressure Fields

Wind and pressure fields were generated utilizing the Oceanweather, Inc. (OWI), Planetary Boundary Layer Model. These wind fields are the required input into the storm surge and wave models for validation and production simulations. The production wind fields were created as part of the JSS analysis (USACE 2008a, USACE 2008b, USACE 2008c). For this study, 40 of the 304 production wind fields were applied to the ADCIRC and UnSWAN modeling system. Further details for storm selection are described in the Appendix D-25 – Risk Assessment Model. Figure 40 displays the ten tracks considered as part of this study. Table 3 lists all 40 storms, with four storms falling on each track.

Table 3 PBL Storm Parameters

Storm Parameters							
Run No.	Wind (m/s)	Pressure (mbar)	Landfall Winds (m/s)	Landfall Pressure (mbar)	Rp (nm)	Track Number	Forward Velocity (kt)
005	52.5	930	41.2	943	17.7	E1	11
006	51.8	930	38.8	951	25.8	E1	11
008	58.4	900	48.4	910	14.9	E1	11
009	57.9	900	46.6	918	21.8	E1	11
014	52.4	930	41.3	943	17.7	E2	11
015	51.7	930	38.9	951	25.8	E2	11
017	58.3	900	48.5	910	14.9	E2	11
018	57.8	900	46.7	918	21.8	E2	11
023	52.3	930	41.5	943	17.7	E3	11
024	51.7	930	38.9	951	25.8	E3	11
026	58.1	900	48.7	910	14.9	E3	11
027	57.7	900	46.8	918	21.8	E3	11
032	52.6	930	41.1	943	17.7	E4	11
033	51.7	930	38.6	951	25.8	E4	11
035	58.1	900	48.3	910	14.9	E4	11
036	57.8	900	46.5	918	21.8	E4	11
041	52.3	930	40.9	943	17.7	E5	11
042	51.8	930	38.3	951	25.8	E5	11
044	58.0	900	48.2	910	14.9	E5	11
045	57.6	900	46.1	918	21.8	E5	11
205	52.5	930	41.2	943	17.7	W1	11
206	51.8	930	38.8	951	25.8	W1	11
208	58.4	900	48.4	910	14.9	W1	11
209	57.9	900	46.6	918	21.8	W1	11
214	52.4	930	41.3	943	17.7	W2	11
215	51.7	930	38.9	951	25.8	W2	11
217	58.3	900	48.5	910	14.9	W2	11
218	57.8	900	46.7	918	21.8	W2	11
223	52.3	930	41.5	943	17.7	W3	11
224	51.7	930	38.9	951	25.8	W3	11
226	58.1	900	48.7	910	14.9	W3	11
227	57.7	900	46.8	918	21.8	W3	11
232	52.6	930	41.1	943	17.7	W4	11
233	51.7	930	38.6	951	25.8	W4	11
235	58.1	900	48.3	910	14.9	W4	11
236	57.8	900	46.5	918	21.8	W4	11
241	52.3	930	40.9	943	17.7	W5	11
242	51.8	930	38.3	951	25.8	W5	11
244	58.0	900	48.2	910	14.9	W5	11
245	57.6	900	46.1	918	21.8	W5	11

Note:

Track Numbers are from Figure 40

Each wind and pressure field includes information for the entire Gulf of Mexico and into the state of Louisiana north to 30.5 degrees latitude. A 15-minute time step was used for all wind fields with a 0.05-degree delta in both the North-South and East-West directions. PBL storm data are mapped onto the ADCIRC mesh geometry during each simulation to apply wind and pressure data at each

node. Wind and pressure data is interpolated linearly in time for ADCIRC and UnSWAN computations occurring between each PBL time step. The nodal wind values are subsequently scaled by the appropriate canopy factor and directional Z_0 value.

The wind surface stress, $\tau_{s\lambda}, \tau_{s\phi}$ is computed by a standard quadratic drag law:

$$\frac{\tau_{s\lambda}}{\rho_0} = C_d \frac{\rho_{air}}{\rho_0} |W_{10}| W_{10-\lambda} \quad (4)$$

$$\frac{\tau_{s\phi}}{\rho_0} = C_d \frac{\rho_{air}}{\rho_0} |W_{10}| W_{10-\phi} \quad (5)$$

W_{10} is wind speed sampled at a 10-meter height over a 10-minute time period (Hsu 1988). The ratio of the density of air to that of water, ρ_{air}/ρ_0 , is 0.001293. The drag coefficient, C_d , is defined by Garratt's drag formula which defines the drag coefficient as a linear function of wind speed (Garratt 1977).

$$C_d = (0.75 + 0.067W_{10}) \times 10^{-3} \quad (6)$$

This drag coefficient is based predominantly on 10-minute averaged wind data. The winds are therefore adjusted to 10-minute averages by noting that shorter averaging periods lead to higher averaged winds and increasing them by a factor of 1.09. This factor leads to almost identical 10-minute winds as would be obtained by converting peak 1-minute winds to 10-minute winds using Powell's recommended conversion factor of 0.89 (Powell et al. 1996). The drag coefficient increases linearly with wind speed to a limit of 0.002 at intermediate winds speeds (18.7 meters per second (m s⁻¹) to 35 m s⁻¹). At higher winds speeds, the linear function is again applied, and is eventually limited to an upper value of 0.003 at wind speeds greater than 45 m s⁻¹ (Figure 41). It is clear from recent literature that there does appear to be an upper limit on the drag coefficient associated with processes such as sheeting (Powell et al. 2003). Upper limit values based on dropsondes are as low as 0.0025 although they may be higher in outer portions of the storm.

Note, the directional changes in surface roughness from open marine conditions do not fully characterize the changes in surface stress on the water column during storm surge inundation. As inundation takes place, the land roughness elements (e.g., marsh grass, crops, and bushes) are slowly submerged and the drag is reduced. Therefore, the overland roughness length is reduced in the model depending upon the local water column height and assuming that the physical roughness height is $30z_{0,land}$ (Simiu and Scanlan 1986). The reduced roughness length $z'_{0,land-directional-k}$ is limited to the marine roughness value, which is reached as the water depth H increases

$$z'_{0,land-directional-k} = z_{0,land-directional-k} - \frac{H}{30} \quad \text{for} \quad z'_{0,land-directional-k} \geq z_{0,marine} \quad (7)$$

where the open marine roughness, $z_{0,marine}$, can be computed based on the Charnock relationship (Charnock 1955) and the relationship between the friction velocity and the applied drag law (Hsu 1988):

$$z_{0_{marine}} = \frac{0.018 C_d W_{10_{marine}}^2}{g} \quad (8)$$

The wind reduction factor, $f_{r-directional-k}$, is then calculated for each of the 12 directions as a ratio between the surface roughness for open marine conditions $z_{0_{marine}}$ and the weighted upwind land roughness adjusted for local inundation. The approximation of the wind speed reduction is based on applying a power law approximation to logarithmic boundary layer theory (Powell et al. 1996, Simiu and Scanlan 1986):

$$f_{r-directional-k} = \left(\frac{z_{0_{marine}}}{z'_{0_{land-directional-k}}} \right)^{0.0706} \quad (9)$$

Actual wind reduction factors used at each node during the simulation are determined from the pre-computed Z_0 directional roughness values closest to the wind direction at that time and place. The adjusted wind speeds used in the wind stress formulae are then computed from PBL marine wind speeds as:

$$W_{10} = f_{r-directional-k} W_{10_{marine}} \quad (10)$$

Future Conditions Model Adjustments

Future conditions were modeled in the study. Year 50 conditions for both the S12 (Moderate Future Conditions) and S13 (Less Optimistic Future Conditions) scenarios were modeled. Details for the S12 and S13 scenarios are described in Appendix C – Environmental Scenarios. In order to account for future conditions in the combined ADCIRC and UnSWAN modeling system, four model components are considered: change in landscape elevation due to subsidence and accretion; vegetation changes; sea level rise (SLR); and consideration of proposed projects.

Model elevation changes are accounted for on the mesh level. *OCPR2012_S50* is used as a basis to create *OCPR2012_S12_G90* and *OCPR2012_S13_G90*. Both G90 mesh versions (S12 and S13) utilize the same mesh nodes, elements and boundaries as *OCPR2012_S50*. Elevation adjustments are made to the model by applying the differences between the current and future conditions DEMs. This is done to ensure that features such as waterways in Figure 12 and pronounced features in Figure 13 are not inadvertently removed, which would occur by directly applying future DEM elevations. Elevation differences are applied using area averaging techniques in the same manner as described in Figure 15. Weir boundary crown elevations are adjusted to account for subsidence as well. Weir elevations defined by recent survey for current conditions, shown in green in Figure 13, are adjusted in the *OCPR2012_S12_G90* and *OCPR2012_S13_G90* meshes by applying elevations provided by the Risk Assessment Team. These areas apply elevations that account for planned levee maintenance. All other weir boundary conditions alter crown elevations by applying the same elevation change to the weir crown that has been applied to the weir base elevation nodes. Thus, the elevation changes that are regionally accounted for in the future DEMs are implemented at the weir boundary conditions as well. Figures 42 through 45 show the resulting *OCPR2012_S12* and *OCPR2012_S13* mesh elevations as well as their differences from the *OCPR2012_S50* mesh elevations.

Vegetation changes are accounted for in the surface characteristics file. Manning’s *n* and *Z₀* values are updated for all nodes where vegetation and land/water characteristics changed using the same process previously described. Areas that were assigned values derived from USGS LU/LC and C-CAP data for current conditions remain static. Eddy viscosity, canopy, and τ_0 values also remain the same for all conditions. The resulting Manning’s *n* and *Z₀* values for *OCPR2012_S12* and *OCPR2012_S13*, as well as their differences from the *OCPR2012_S50* frictional characteristics are shown in Figures 46 through 57. A detailed description of the surface characteristics methodology is contained in Section 1e, Description of Input Data: Current Conditions (Year 0+1 day) Surface Characteristics.

The inclusion of SLR varies with model initial conditions. The S50 initial condition is increased based on the level of eustatic SLR being analyzed. For instance, S12 experiences 0.89 feet of SLR, rendering a model initial condition of 2.09 feet NAVD88. Details for S50, S12 and S13 are found in Table 4. This initial condition is applied throughout the model domain.

Table 4 Model Initial Conditions Including Sea Level Rise

Scenario	Model Initial Condition (NAVD88 m)	Model Initial Condition (NAVD88 ft)	Sea Level Rise (ft)
S50	0.37	1.20	0.00
S12	0.64	2.09	0.89
S13	0.82	2.68	1.48

Proposed projects are included in the future with plan (FWP) ADCIRC meshes. Thirty-four coastal protection projects are considered in this analysis. These 34 projects are grouped into seven ADCIRC meshes in order to analyze multiple independent projects with one mesh, saving on computational cost by simulating 40 storms per mesh rather than per project. The project groupings were constructed in a manner such that the projects do not interfere with the response of an adjacent project. This was confirmed during the quality control portion of the study, described in Section 1e. Figures 58 through 64 display the mesh groupings. For naming convention purposes, mesh grouping 1 is referred to as G91, mesh grouping 2 is referred to as G92, etc. Table 5 contains a list of project attributes for all 34 coastal protection projects analyzed. All seven future with project mesh groupings were simulated using the same mesh elevation and surface characteristics as the *OCPR2012_S12_G90* and *OCPR2012_S13_G90* simulations. Future projects were implemented by inserting a new weir boundary condition along the project alignment or updating the crown elevation of existing weir boundary alignments. Crown elevations are listed in Table 5.

Table 5 Project Attributes

Project Name	Project Mesh Number	Modeled Elevation (ft)	Lift Amount (ft)
001.HP.07	G91	33.0	N/A
002.HP.07	G91	8.0	N/A
03b.HP.07	G91	18.0	N/A
004.HP.05	G91	9.0	N/A
004.HP.11	G91	14.4	N/A
001.HP.05	G92	13.5	N/A
001.HP.09	G92	30.3	N/A

Table 5 Project Attributes

Project Name	Project Mesh Number	Modeled Elevation (ft)	Lift Amount (ft)
002.HP.01	G92	9.5	N/A
03a.HP.02a	G92	12.0-28.0	N/A
03b.HP.12	G92	16.5	N/A
004.HP.03	G92	9.0	N/A
004.HP.06	G92	17.0	N/A
001.HP.04	G93	15.0-35.0	N/A
002.HP.06	G93	15.5	N/A
03b.HP.10	G93	13.5	N/A
004.HP.12	G93	21.4	N/A
001.HP.13	G94	15.4	N/A
002.HP.05	G94	12-16.5	N/A
03b.HP.06	G94	21.5	N/A
002_HP_09	G94	N/A	2.43
001.HP.02	G95	31.5	N/A
002.HP.04	G95	14.0-17.0	N/A
03b.HP.09	G95	16.5	N/A
004.HP.04	G95	17.0-20.0	N/A
Larose_GoldenMeadow_Lift	G95	N/A	2.76
001.HP.08	G96	24.5	N/A
03b.HP.08	G96	18.0	N/A
004.HP.13	G96	12.0	N/A
002_HP_08	G96	N/A	2.23
001.HP.01	G97	33.0	N/A
03a.HP.02b	G97	19.5-36.5	N/A
03b.HP.11	G97	18.0	N/A
004.HP.14	G97	15.0	N/A
001_HP_20	G97	N/A	2.23

Note: Incorrect alignments were modeled for 001.HP.09 and 002_HP_09; please disregard modeled output in these areas.

e. Description of Output Data

The ADCIRC and UnSWAN models calculates storm surge, water currents, wave height, wave period and wave direction at every node in the mesh at every time step. At the end of each simulation, the model creates output files which contain time series information for these parameters, as well as the maximum value at any given time step during the simulation. The only exception comes in the form of the wave period. The maximum wave period is synced to the time in which the maximum significant wave height occurs. For quality control purposes, time series and maximum data are analyzed for each storm and each scenario. However, ultimately data at specific locations is passed to the Risk Assessment Model.

The output passed to the Risk Assessment Model consists of maximum values for surge, wave height, and wave period as well as hydrographs detailing the evolution of surge. These hydrographs are output every 15 simulation minutes. There are four different point sets: Unprotected Census

Blocks, Semi-Protected Census Blocks, Regularly Spaced Points, and Surge/Wave Points. Unprotected Census Blocks, Semi-Protected Census Blocks and Surge/Wave points were determined by the Risk Assessment Model. Regularly spaced points were created by the Storm Surge/Waves Team at 2.5 kilometer intervals across the state to be used for mapping purposes. The Risk Assessment Model utilizes maximum surge and maximum wave height information for all point sets. At the Surge/Wave Points, wave period and hydrograph data were additionally supplied.

For the purposes of illustration, images of synthetic storms 009 and 227 are shown for the S50, S12_G90, and S13_G90 project simulations. A comprehensive set of figures, illustrating the surge and wave results for all of the synthetic storms simulated for S50, S12_G90, and S13_G90, are included in Appendices D-24-B, D-24-C, and D-24-D, respectively.

Current Conditions

Simulation results were analyzed on the current conditions (*OCPR2012_S50*) mesh to ensure model stability and performance, validate the model, as well as to establish surge responses for comparison to the future scenarios. The mesh was created using current data sources for bathymetry and topography, and model parameters were assigned using current land cover (frictional resistance to flow), directional roughness length, forested canopy, and eddy viscosity data, as described in Section 1d. Maximum water surface elevation, maximum significant wave height, peak wave period and wave direction were examined for current conditions simulations. For the purposes of illustration, images of maximum water surface elevation and maximum significant wave height for synthetic storms 009 and 227 are shown in Figures 65 through 76.

S12_G90

The model mesh elevation and frictional parameters were modified using the methodology outlined in Section 1d. Simulations were performed on the S12_G90 future without action mesh. For the purposes of illustration, images of maximum water surface elevation and maximum significant wave height for synthetic storms 009 and 227 are shown in this section. Results of S12_G90 maximum water surface elevation for storms 009 and 227 are illustrated in Figures 77 through 82. Figures 83 through 88 show the difference in maximum water surface elevation between 2011 current conditions (S50) and S12_G90. There is a region-wide water surface elevation increase compared to S50, due to the increase in the initial water level of the simulation to account for SLR. Surge generally propagates further inland compared to S50. Offshore, the rise in surge takes on the value of sea level rise. However, the rise in surge inland is nonlinear, with localized increases in surge response as high as two or three times the sea level rise value.

Comparisons of maximum wave height were made between S12_G90 and S50. Figures 89 through 92 show the maximum significant wave height for storms 009 and 227, while Figures 93 through 96 show the difference in maximum water surface elevation as compared to S50 current conditions. Significant wave heights exhibit an increase of over four feet at some barrier islands and headlands, and wave heights are generally one to two feet higher across much of the study area, as compared to current condition waves. One notable exception is that waves appear to decrease by about one foot in the vicinity of the Atchafalaya and Wax Lake Outlet Deltas. This decrease is due to the accretion that occurs in the area.

Hydrograph plots were also produced for the surge and wave points shown in Figure 36. Six of those points are presented here for illustrative purposes. Figure 97 shows the location of the six

hydrograph locations plotted. Note that none of the hydrographs are in Southwestern Louisiana, as existing infrastructure does not exist that requires hydrograph output for risk and damage assessment purposes for current and future without action studies. Therefore, hydrograph information was not output by the ADCIRC model for surge and wave points shown in Southwestern Louisiana in Figure 36. Figures 98 and 99 show example hydrographs at the six output locations for storms 009 and 227, respectively. S12_G90 output is compared to S50 in order to analyze the effects of SLR, subsidence, accretion and vegetation change throughout the duration of the storm.

S13_G90

The model mesh elevation and frictional parameters were modified using the methodology outlined in Section 1d. Simulations were performed on the S13_G90 future without action mesh. For the purposes of illustration, images of maximum water surface elevation and maximum significant wave height for synthetic storms 009 and 227 are shown in this section. Results of S13_G90 maximum water surface elevation for storms 009 and 227 are illustrated in Figures 100 through 105. Figures 106 through 111 show the difference in maximum water surface elevation between 2011 current conditions (S50) and S13_G90. There is a greater region-wide water surface elevation increase than both S50 and S12_G90, due to increased initial water level of the simulation to account for the S13 SLR. Surge generally propagates further inland compared to S50 and S12_G90. Similar to S12_G90, the increase in storm surge values are approximately the SLR value offshore and vary nonlinearly in coastal Louisiana.

Comparisons of maximum wave height were made between S12_G90 and S50. Figures 112 through 115 show the maximum significant wave height for storms 009 and 227, while Figures 116 through 119 show the differences in maximum water surface elevation as compared to S50 current conditions. Significant wave heights exhibit an increase of over four feet at some barrier islands and headlands, and wave heights are generally one to two feet higher across much of the study area, as compared to current conditions waves. Waves generally propagate inland farther than S50 or S12_G90. One notable exception is that waves appear to decrease by about one foot in the vicinity of the Atchafalaya and Wax Lake Outlet Deltas.

Hydrograph plots were also produced for the same six points shown in Figure 97. Figures 120 and 121 show example hydrographs at the six output locations for storms 009 and 227, respectively. S13_G90 output is compared to S50 in order to analyze the effects of SLR, subsidence, accretion and vegetation change throughout the duration of the storm.

S12 Future with Project (G91-G97) Simulations

The impacts of projects on S12 were evaluated using Project Meshes G91, G92, G93, G94, G95, G96, and G97, shown in Figures 58 through 64. A comprehensive set of results images for all seven project meshes is contained in Appendix D-24-C. Results of storms 009 and 227 on the S12 project mesh 6 (S12_G96) are presented in this section. Figures 122 through 127 show the difference in maximum water surface elevation between S12_G96 and S12_G90. These results illustrate that, in general, surge accumulates on the unprotected side of proposed projects, and is decreased on the protected side. This can be seen in Figure 127, using the Pontchartrain Barrier alignment as an example. Surge is amplified across a wide area outside of the protection feature, affecting St. Bernard Parish, the East Bank of Plaquemines Parish, and the Pearl River Basin of St. Tammany Parish. The structure provides over four feet of surge attenuation throughout the Pontchartrain Basin on the protected side, as shown at station 191 in the hydrographs in Figures 128 and 129

comparing S12_G90 with S12_G96. Similar effects are seen on significant wave height, as shown in Figures 130 through 133. An important note is that depending on the storm track, certain protection features can increase surge on the protected side of projects. An example of this is shown in Figure 123. Alignment 004.HP.13 experiences winds that increase surge on the protected side of the project.

S13 Future with Project (G91-G97) Simulations

The impacts of projects on S13 were evaluated using Project Meshes G91, G92, G93, G94, G95, G96, and G97, shown in Figures 58 through 64. A comprehensive set of results images for all seven project meshes is contained in Appendix D-24-D. Results of storms 009 and 227 on the S13 project mesh 6 (S13_G96) are presented in this section. Figures 134 through 139 show the difference in maximum water surface elevation between S13_G96 and S13_G90. These results illustrate that, in general, surge accumulates on the unprotected side of proposed projects, and is decreased on the protected side. This can be seen in Figure 138, using one of the Southwest Coastal Levee alignments as an example. Surge is amplified across a wide area outside of the protection feature, affecting much of the coastal Chenier Plain with up to three feet of increased surge height. The structure provides over four feet of surge attenuation on the protected side. A similar change in hydrograph response as S12 can be seen in Figures 140 and 141. Additionally, similar changes as S12 are seen on significant wave height, as shown in Figures 142 through 145.

QA/QC Process

The QA/QC process for the model output consists of two steps, product creation and product review. Product creation is further broken down into three main categories: 1) maximum water surface elevation (WSE) plots; 2) UnSWAN wave results (maximum wave height and corresponding wave period and direction); and 3) difference plots comparing base conditions with project conditions. In order to maintain consistency among the products, an automated script is used in the creation of these products. One script plots the maximum WSE and UnSWAN wave period and wave height results using the same seven zooms shown in Figure 146. Another script searches through the 40 storms and calls the plotting script when the simulation has completed. This minimizes the amount of human error that can be introduced in grabbing the correct output file since the script automatically searches through the storms that remain to be plotted and captures the appropriate files. A similar calling script is used to create difference files for the WSE and UnSWAN results (project less future without action; e.g. S12_G94_V00 less S12_G90_V00) and plot these differences using symmetric scales centered at zero.

For the WSE and UnSWAN wave output created for any given storm in the 40 run suite, plots are created for the following seven zooms:

- z1 – the Louisiana Gulf coast
- z2 – the western study region
- z3 – the eastern study region
- z4 – close-up view of western inland region
- z5 – close-up view of central inland region
- z6 – close-up view of eastern inland region

z7 – close-up of the Mississippi River Delta.

These are also shown in Figure 146. Note that all of the smaller zooms overlap the larger zooms to provide complete coverage of the study area. However, for the difference plots, only the first three zooms are created. The main goal of the difference plots is to verify that a project's area of influence makes sense and to double-check that project data was properly implemented. The majority of these plots should be white, indicating zero difference between the FWOA scenario and the project scenario.

After the plots have been created, they undergo a thorough review. The UnSWAN wave plots are reviewed by a wave expert and the maximum WSE plots are reviewed by two hydrodynamics experts. The WSE plots are examined for unnatural "mounds" of water due to numerical artifacts, proper input of river flow rates, and hydraulic area of influence for projects. Further examination of the hydraulic area of influence for the proposed project is conducted by examining the difference plots of WSE. It is expected that the only areas of non-zero difference should be in the immediate vicinity of the proposed project. Differences can be negative or positive indicating that surge is either reduced (or eliminated entirely) or accumulation is occurring along new levees. The creation and review process occurs concurrently with the production runs so that any errors can be quickly corrected and the production runs halted and resubmitted.

The current condition ADCIRC and UnSWAN wave plots are reviewed and compared to JSS study results and make sure both results are consistent and physically reasonable, including wave propagation, shoaling and dissipation. In the JSS analysis, although the wave model STWAVE was used, the wave results should be in the same order of magnitude because the UnSWAN model is equivalent to the STWAVE with full-plane mode. There are some differences between UnSWAN and STWAVE in half-plane mode, especially for the wave field behind barrier islands, since STWAVE with half-plane mode is unable to resolve the offshore wave propagation. In the nearshore and overland area, most of waves are depth-limited, resulting in similar UnSWAN and STWAVE results.

Post Processing and Transferring Output to Risk Assessment Model

Four sets of data points were constructed by the Risk Assessment Team for output from the storm surge and wave models. These points were:

1. Surge/Wave Points (Figure 36)
2. Semi-Protected Census Blocks (Figure 37)
3. Unprotected Census Blocks (Figure 38)
4. Regularly Spaced Points (Figure 39)

This data is broken down into two types; time series data and maximum value data. Maximum surge values are the maximum water surface elevation at a given location at any time during the simulation. Maximum wave values consist of the maximum significant wave height at a location at any time during the simulation and the corresponding peak period. This means that at the time the maximum wave height occurred, the computed peak period is saved from that time. Time series data consists of water surface elevations written during the simulation every simulation half hour at specified locations. The types of data provided for each dataset is summarized in Table 6.

Table 6 Data Types passed at Various Point Sets to Risk Assessment Team

	Max Surge	Time Series Surge	Max Wave Height	Peak Period
Unprotected Census Blocks	✓		✓	
Semi-Protected Census Blocks	✓		✓	
Surge/Wave Points	✓	✓	✓	✓
Regularly Spaced Points	✓		✓	

Hydraulic Sub Units

Due to the limited selection of storms used, responses at some points throughout the state were limited, exaggerating the statistical extrapolation used to compute surge for many other storms. In order to make for a more accurate risk and damage assessment, points with limited responses were checked to see if they were candidates for a nearest neighbor value based upon the hydraulic sub units and associated criteria.

Hydraulic sub units were created using the known features of the state and the ADCIRC model to create polygons of areas hydraulically connected, with respect to storm surge. Figures 147 through 154 show what the polygons look like after they were created. Each color represents a particular sub unit. Geoprocessing software was used to compute which hydraulic sub unit each output location fell within. Different sets of sub units were created from each project mesh as certain protection projects might hydraulically disconnect areas that were once connected.

The criteria used to determine if a point should use a nearest neighbor value relied on the number of times a storm was able to wet a location for a particular storm track. If an output point was wet or dry for all for storms that fell on a particular track, then the point was left untouched. If between one and three storms wet a point, then the nearest wet point within the sub unit for the storm was determined and added in place of the null value. Points outside of the hydraulic sub unit were not considered. If all other points within the sub unit were also dry for that particular storm, no action was taken. The nearest neighbor value was allowed to be pulled from any dataset to find the most accurate substitution value that could be calculated within a reasonable amount of time.

f. Statement on the Capabilities and Limitations of the Model

ADCIRC solves the depth-averaged shallow water equations using an unstructured finite element approach. Derivations of the shallow water equations require making the following assumptions:

- The flow is incompressible which is appropriate for fluids such as liquid water;
- The pressure distribution through the water column is linear with depth (hydrostatic);
- Boussinesq approximation to neglect density differences in all terms except those involving the gravity term;
- Horizontal velocity is independent of depth; and
- Horizontal motions are much greater than the vertical motions.

These assumptions mathematically justify depth averaging of the Navier-Stokes Equations, which are an expression of mass and momentum conservation for fluid flow. The depth averaged Navier-

Stokes equations are called the shallow water equations. With the above approximations, the shallow water equations describe horizontally dominant flows such as oceanic tides, wind driven storm surge, circulation in estuaries, bays, and lakes and flow in rivers. The formulation used in ADCIRC also includes terms to account for Coriolis accelerations, variations in atmospheric pressure at the water surface, viscous dissipations and frictional resistance (drag) from the roughness of the surface over which the water flows.

The viscous term can be used to account for molecular diffusion of momentum and the much larger dissipation due to turbulent mixing. While many sophisticated turbulence models exist in the scientific literature, ADCIRC uses a very simple approximation for turbulent dissipation. ADCIRC uses a scalar eddy viscosity in place of molecular viscosity.

The shallow water equations are non-linear partial differential equations which are not easily solved in closed form using standard tools of calculus. Numerical approximations are required to solve the equations. The ADCIRC model uses linear, triangular finite element method to approximate the spatial derivatives in the equations and a variably implicit finite-difference scheme to replace the time derivatives. The basic derivation of the shallow water equations is called the primitive form, which produces errors when solved with linear finite elements. In order to overcome these numerical difficulties with linear finite elements, ADCIRC takes advantage of a reformulation of the shallow water equations in which the equations are recast into a wave equation formulation. The specific details of the formulation are described in the theory section of this report. The beneficial outcome of reformulating the equations is that the ADCIRC model is robust and stable.

ADCIRC is open-source and widely distributed. It has been in use for more than 30 years by university researchers, the U.S. Army Corps of Engineers, FEMA, state governments, and consulting firms around the world. ADCIRC has been deployed successfully on many computer systems from single processor desktop PCs to multi-processor super computers. There is an active development community in which the latest advances are tested and compiled. The strength of development across a diversity of computer platforms and by a large group of participants is a flexible, well exercised model, that has been extensively verified and validated for a large number of flow scenarios.

The fidelity of an ADCIRC solution depends upon the quality and accuracy of the model input. The user of the ADCIRC computer program must supply the finite element mesh. The mesh is actually a model of the terrain and roughness over which the flow occurs. The user creates a mesh of non-overlapping triangles for which the vertices of the triangles are called nodes. The mesh can be constructed in geographic coordinates or a Cartesian coordinate system such as State-Plane coordinate systems. At each node, an elevation of topography/bathymetry and frictional parameters are defined. When the ADCIRC code is run to solve the flow across a mesh, it uses the same mesh to resolve the flow features such as velocity gradients, circulation, and eddies in the flow. Thus, the size, spacing, and configuration of the mesh dictate the solution accuracy. The user can control the accuracy through the size of the elements in the mesh; the smaller the elements are, the more detail can be resolved both in the underlying terrain and in the flow field. However, as the element size decreases, it requires more elements and nodes to cover the same spatial extent. Because the solution time required for the ADCIRC code to solve the governing equations is proportional to the total number of nodes in the mesh, the cost of running the ADCIRC model increases as element size decreases. This is a limitation that ADCIRC shares with all computer models; increasing accuracy comes with increasing cost to run the code. One of the strengths of the

unstructured mesh used with ADCIRC is that the element size can vary substantially throughout a mesh. The user can define small elements where needed and can use large elements where the bathymetry or flow features vary gradually in space. See Figures 6 through 9 for examples of how the element size varies to resolve topographic features over many horizontal scales. This allows ADCIRC users to balance accuracy and efficiency.

Efficiency is also enhanced by virtue of attention to optimization and solution routines. ADCIRC has been optimized by unrolling loops for enhanced performance on multiple computer architectures. ADCIRC includes MPI library calls to allow it to operate at high efficiency (typically better than 90 percent) on parallel computer architectures. The solution method allows some flexibility for the user to choose the solution procedure. The equations can be solved using either a consistent or a lumped mass matrix (via a compiler flag) and an implicit or explicit time stepping scheme (via variable time weighting coefficients). If a lumped, fully explicit formulation is specified, no matrix solver is necessary. In all other cases the Generalized Wave-Continuity Equation (GWCE) is solved using the Jacobi preconditioned iterative solver from the ITPACKV 2D package. When ADCIRC is run with the explicit formulations which do not require a matrix solver, the code is very efficient and fast. In addition, ADCIRC makes use of a least squares analysis routine that computes harmonic constituents for elevation and depth averaged velocity during the course of the run, thereby avoiding the need to write out long time series for post processing.

ADCIRC users are required to define boundary conditions at the edges of the mesh. Boundary conditions allow the solution with the computational domain to be consistent with conditions external to the domain. Boundary conditions also provide a mechanism to introduce mass and momentum sources, such as riverine discharge entering the computational domain. ADCIRC users can specify any of the following boundary conditions along segments of the domain boundary:

- specified elevation variation (harmonic tidal constituents or time series);
- specified normal flow (steady or time varying);
- zero normal flow;
- slip or no-slip conditions for velocity;
- external barrier overflow out of the domain;
- internal barrier overflow between sections of the domain;
- surface stress (wind and/or wave radiation stress);
- atmospheric pressure; and
- outward radiation of waves (Sommerfield condition).

Of particular interest to solving storm surge flood conditions is the use of the internal and external barrier boundary conditions. These conditions are used to provide ADCIRC with the capability of solving flow over weirs and levees.

For flow scenarios that include the effect of tides, ADCIRC has the capability of defining tidal constituents for all relevant celestial forcing, internal tides and tidal potential effects.

ADCIRC has a lot of flexibility in allowing the user to save model results in a number of formats. The user can choose between ASCII, binary, or NetCDF formats for time series of the solution or other state variables at defined locations or global solution values. Harmonic parameters may also be produced.

One uncertainty that should be noted is the dependency of mesh quality upon the available data. The elevations in the mesh are only as accurate as the topographic and bathymetric data. The friction parameters are only as accurate as the land cover data sets used to derive them.

The ADCIRC model also has the capability to be coupled to a separate surface wave model to account for the additional wave setup associated with the wave conditions created during a hurricane event. For the work described here, ADCIRC was coupled to the unstructured SWAN model. Unstructured SWAN is a derivative of the structured SWAN model (described in detail in Section 2a) which has been modified to use the same finite element mesh as the ADCIRC model. UnSWAN is a spectral wave model which solves the propagation, growth and decay of wave energy for waves of different frequencies. UnSWAN accounts for wave growth due to winds, energy lost to whitecapping, wave breaking, and bottom frictions, and energy exchanged between wave interactions. When waves break, some of the momentum they lose is transferred to the water column which creates additional push on the water and can increase surge by as much as two or three feet. UnSWAN exports wave radiation stress gradients which ADCIRC incorporates as an additional nodal forcing in the momentum balance.

Summary

Following are the primary capabilities of the ADCIRC and UnSWAN model:

1. The finite element mesh provides a detailed model of topography, bathymetry and frictional roughness for the region of interest.
2. The topography in the model resolves hydraulically relevant levees, roads, railroads, ridges, spoil mounds and islands.
3. The bathymetry resolves elevations from off shore to interior bays, lakes, bayous, natural and dredged channels, rivers and canals.
4. The frictional parameters are derived from the most recent land cover data and from future land cover forecasts provided by USGS (Appendix D-2 – Wetland Morphology Model), the Vegetation Model (Appendix D-4 – Vegetation Model) and C-CAP.
5. The finite element mesh utilizes the large domain paradigm with local resolution. This paradigm simplifies specification of boundary conditions, and accurately captures large basin scale effects and basin-to-basin interactions, while simultaneously capturing important small scale topographic and flow features with localized high resolution.
6. Unstructured meshes provide flexibility to meet accuracy requirements and efficiency/time constraints.
7. The governing equations solved by the ADCIRC code are appropriate for describing tides, riverine flow, channel flow, wind driven storm surge, surge attenuation by friction and topography, surge modification by wave setup and inland inundation by propagating surge.

8. The ADCIRC code accounts for modification of the computed flow by Coriolis, turbulent dissipation, frictional dissipation, atmospheric pressure/wind, tidal potential Earth self-potential tides.
9. ADCIRC makes use of elevation, flow and radiation boundary conditions.
10. The solution algorithm is robust, second-order, non-damped and consistent with the governing equations.
11. The ADCIRC code is well documented and has been subjected to 30 years of peer-review, testing and validation exercises.
12. ADCIRC and UnSWAN are dynamically coupled and use the same finite element mesh.
13. The governing equations solved by the UnSWAN code are appropriate for describing wave growth by wind, wave attenuation by bottom friction, whitecapping, and breaking and wave-wave interactions.
14. The coupling to ADCIRC allows UnSWAN to make use of time variation in water column depth and inundation during a simulation.
15. The coupling to UnSWAN allows ADCIRC to include the contribution of surface waves to the momentum balance for the entire water column and thereby include wave-setup.
16. The coupled ADCIRC and UnSWAN model has been optimized to run efficiently on massively parallel platforms such as those used for this study.

Following are potential limitations of the ADCIRC and UnSWAN models, though none are considered necessary to accurately propagate storm surge and waves:

1. ADCIRC includes the approximations used to derive the shallow water equations.
2. No three dimensional effects are included.
3. Neither variation in density or density gradient effects are considered.
4. No propagation of sound waves or other compressibility effects are considered.
5. Thermal, saline and sediment transport are neglected.
6. UnSWAN is a spectral model thus does not resolve individual waves.
7. ADCIRC and UnSWAN depend upon the finite element mesh adequately resolving all hydraulically relevant topographic flow features.
8. ADCIRC and UnSWAN depend upon the finite element mesh being adequately resolved to obtain the level of accuracy required from the project.
9. ADCIRC and UnSWAN depend upon the accuracy of the underlying data sources for topography, bathymetry, levee heights and land cover.
10. ADCIRC and UnSWAN output accuracy depends upon the accuracy of the hurricane wind and pressure input.

g. Description of Model Development Process Including Documentation on Testing Conducted (Alpha and Beta tests)

ADCIRC was selected as the basis for the surge modeling effort. This model has been and continues to be a standard coastal model utilized by the USACE, NOAA and other agencies. ADCIRC has been in development for over 30 years and is in continual development by the larger ADCIRC user group. Alpha and beta tests are conducted for each ADCIRC version prior to public release.

UnSWAN has been selected due to its ease of coupling with ADCIRC. UnSWAN is included in the ADCIRC version 49 code and has been rigorously validated and compared to similar spectral wave model such as structured SWAN and STWAVE (Dietrich 2011a, Dietrich 2011b).

The *OCPR2012* mesh was tested during the validation stage, described in Section 3d. Initial validation exercises were completed using a model with elevation and frictional parameters mapped from the SL18 model. After including revised elevation data and updated land cover data, multiple tests were conducted to ensure that SL18 parameters applied to the *OCPR2012* mesh, particularly for land cover types supplied by USGS (Appendix D-2 – Wetland Morphology Model) and the Vegetation Model (Appendix D-4) that did not exist in the C-CAP data used to create the SL18 model. The final mapping of Manning’s n and Z_0 values assigned from land cover are described in Table 2. These values were similar to those of the SL18 model and produced the best results when hindcasting Hurricanes Gustav and Ike.

2. Technical Quality

a. Theory

The ADCIRC theory for this study remains largely the same as that of the JSS analysis. Theory described in those documents is below (USACE 2008a, USACE 2008b, USACE 2008c).

ADCIRC can be run either as a two-dimensional depth integrated (2DDI) model or as a three-dimensional (3D) model. In either case, elevation is obtained from the solution of the depth-integrated continuity equation in GWCE form. Velocity is obtained from the solution of either the 2DDI or 3D momentum equations. All nonlinear terms have been retained in these equations.

ADCIRC-2DDI, the two-dimensional, depth-integrated implementation of the ADCIRC coastal ocean model, was used to perform the hydrodynamic computations in this study (Luettich et al. 1992, Westerink et al. 1992, Westerink 1993, Luettich and Westerink 2004). The model uses the depth-integrated barotropic equations of mass and momentum conservation subject to the incompressibility, Boussinesq, and hydrostatic pressure approximations. The primitive, non-conservative continuity and momentum equations are given below in a spherical coordinate system (Kolar et al. 1994, Luettich and Westerink 1995).

$$\frac{\partial \zeta}{\partial t} + \frac{1}{R \cos \phi} \left(\frac{\partial UH}{\partial \lambda} + \frac{\partial (VH \cos \phi)}{\partial \phi} \right) = 0 \quad (11)$$

$$\begin{aligned} & \frac{\partial U}{\partial t} + \frac{1}{R \cos \phi} U \frac{\partial U}{\partial \lambda} + \frac{V}{R} \frac{\partial U}{\partial \phi} - \left(\frac{\tan \phi}{R} U + f \right) V \\ & = -\frac{1}{R \cos \phi} \frac{\partial}{\partial \lambda} \left[\frac{p_s}{\rho_0} + g(\zeta - \alpha \eta) \right] + \frac{v_T}{H} \frac{\partial}{\partial \lambda} \left[\frac{\partial UH}{\partial \lambda} + \frac{\partial UH}{\partial \phi} \right] + \frac{\tau_{s\lambda}}{\rho_0 H} - \tau_* U \end{aligned} \quad (12)$$

$$\begin{aligned} & \frac{\partial V}{\partial t} + \frac{1}{R \cos \phi} U \frac{\partial V}{\partial \lambda} + \frac{V}{R} \frac{\partial V}{\partial \phi} + \left(\frac{\tan \phi}{R} U + f \right) U \\ & = -\frac{1}{R \cos \phi} \frac{\partial}{\partial \phi} \left[\frac{p_s}{\rho_0} + g(\zeta - \alpha \eta) \right] + \frac{v_T}{H} \frac{\partial}{\partial \phi} \left[\frac{\partial VH}{\partial \lambda} + \frac{\partial VH}{\partial \phi} \right] + \frac{\tau_{s\phi}}{\rho_0 H} - \tau_* V \end{aligned} \quad (13)$$

where:

- t = time;
- λ, ϕ = degrees longitude and latitude;
- ζ = free surface elevation relative to the geoid;
- U, V = depth-averaged horizontal velocities;
- H = $\zeta + h$ = total water column;
- h = bathymetric depth relative to the geoid;
- f = $2\Omega \sin \phi$ = Coriolis parameter;
- Ω = angular speed of the Earth;
- p_s = atmospheric pressure at the free surface;
- g = acceleration due to gravity;
- η = Newtonian equilibrium tide potential;
- α = effective Earth elasticity factor;
- ρ_0 = reference density of water;
- $\tau_{s\lambda}, \tau_{s\phi}$ = applied free surface stress;
- $\tau_* = C_f \frac{(U^2 + V^2)^{1/2}}{H}$ = bottom friction term;
- C_f = nonlinear bottom friction coefficient; and
- v_T = depth averaged horizontal eddy viscosity coefficient.

A practical expression for the Newtonian equilibrium tidal potential, η , is given by Reid (1990).

Numerical solutions to the shallow water equations on unstructured meshes using finite element methods have been under development for the past 30 years (Westerink and Gray 1991, Kolar and Westerink 2000). Unstructured finite element-based methods permit shallow water equation solutions that can localize resolution leading to globally and locally more accurate solutions within the realm of feasible computational expense. A significant problem for unstructured shallow water equation solutions has been avoiding non-physical spurious modes with wavelengths nearly twice

the mesh size without requiring adding artificial damping. The artificial spurious modes are related to a numerical dispersion curve which leads to dual wave numbers for one frequency in the forcing spectrum. The analytical dispersion curve for the shallow water equation is monotonic. Four finite element-based unstructured shallow water equation algorithms have emerged which are at least second order accurate in space, have noise free solutions without requiring artificial damping, and are sufficiently robust to be applied to the wide range of scales of motion and wide range of hydrodynamic balances that exist when computing flows in the deep ocean to computing flows in inlets, floodplains, and rivers. These algorithms include the GWCE formulation (Lynch and Gray 1979, Kinnmark 1986, Kolar and Westerink 2000), the Quasi-Bubble (QB) formulation (Galland et al. 1991); Raviart-Thomas based solutions, and recently the Discontinuous Galerkin Method (Dawson et al. 2006, Kubatko et al. 2006a, Kubatko et al. 2006b, Kubatko et al. 2007). The most mature of these algorithms are the GWCE and the QB formulations, which are, in fact, functionally almost identical despite entirely different approaches to deriving them (Atkinson et al. 2004). It is the GWCE solution that we have selected as our current base algorithm in our shallow water equations code, ADCIRC (Luettich et al. 1992, Westerink et al. 1992, Westerink 1993, Luettich and Westerink 2004). The GWCE is generated by combining the spatially differentiated momentum equation in its conservative form with the temporally differentiated continuity equation and adding the continuity equation multiplied by a numerical parameter τ_0 (Kinnmark 1986, Kolar and Westerink 2000). The τ_0 parameter in fact controls the dispersion properties of the solution and its optimal selection avoids a folded dispersion curve and optimizes phase propagation properties. Extensive numerical experimentation and comparisons to the functionally equivalent QB finite element (FE) solution provide guidance in the specification of the τ_0 parameter as (Kolar et al. 1994, Atkinson et al. 2004):

$$\tau_0 = \frac{i\omega + 4\tau_*}{3} \quad (14)$$

where ω equals the forcing frequency.

The friction term τ_* increases as depth decreases and a higher τ_0 is required in shallow, nearshore regions (generally less than 30 feet deep); a smaller value is more appropriate in deep basins.

However, τ_* is also proportional to the flow velocity. Therefore, it is also important to apply larger τ_0 values in high-flow regions that can be deep, such as rivers and inlets. Operationally, we have implemented our GWCE solution to accommodate spatially variable τ_0 and set $\tau_0 = 0.005$ in quiescent waters deeper than 30 feet outside of Southern Louisiana and Mississippi, we set $\tau_0 = 0.02$ in waters shallower than 30 feet outside of Southern Louisiana and Mississippi, and we set $\tau_0 = 0.03$ in waters shallower than 30 feet and/or in rivers and inlets where higher velocities lead to higher frictional resistance within Southern Louisiana and Mississippi (Feyen et al. 2000). In addition, we increase τ_0 within Southern Louisiana and Mississippi based on the total water column height and local currents:

$$\tau_0 = 0.02 + \frac{4\tau_*}{3} \quad (15)$$

This automated current dependent value optimizes both accuracy and robustness, particularly for the very high current speeds encountered during hurricanes.

The GWCE and the momentum equations are solved sequentially. The FE solution is implemented using Lagrange linear finite elements in space and three and two level schemes in time for the GWCE and momentum equations, respectively. Details of the discretization and solution techniques used in ADCIRC are given in Luettich et al. 1992, Westerink et al. 1992, Westerink 1993, Luettich and Westerink 2004. The present simulations were done using an implicit discretization for all linear and some nonlinear terms in the equations and an explicit discretization for most nonlinear terms. This effectively imposes a Courant restriction on the time stepping solution. However, because GWCE

solutions are always more accurate for a Courant number, $C = \frac{\sqrt{gh\Delta t}}{\Delta x}$, below unity and because our wetting/drying procedure is Courant limited as well, this condition is not restrictive.

Modeling storm surge inundation requires that the model accurately represent wetting and drying processes at the mesh scale. ADCIRC applies a wet/dry algorithm that is based on a combination of nodal and elemental criteria (Luettich and Westerink 1999, Dietrich et al. 2005). The algorithm requires all nodes within an element to be wet in order for that element to be included in the hydrodynamic computations. Two parameters are used to define the wetting/drying criteria. First, H_0 defines the nominal water depth for a node to be considered wet. Second, a minimum velocity U_{min} is specified that must be exceeded for water to propagate from a wet node to a dry node. Nodes are defined as initially dry if they lie above the defined starting water level or if they are below the starting water level but are within pre-defined regions, such as ring levees (e.g., New Orleans).

The algorithm proceeds through the following steps to update the wet and dry elements for the next time level. Wetting is accomplished by examining each dry element with at least two wet nodes with depth greater than $1.2 H_0$ (ensuring sufficient water depth to sustain flow to the adjacent node). The velocity of the flow from the wet nodes toward the dry node along each element edge is computed based on a simple force balance between the free surface gradient and the bottom friction. If this velocity exceeds U_{min} , then the third node and the element are wetted. Finally, a check is made for elements that are surrounded by wet elements to ensure sufficient water column height (greater than $1.2 H_0$ at all flow originating nodes) to allow flow to occur through these elements. While a purely nodal wetting scheme will allow these elements to wet, the elemental check may prevent this from occurring. For hurricane storm surge inundation, wet/dry parameters that are relatively unrestrictive have been found to be most effective: $H_0 = 0.10$ m, and $U_{min} = 0.01$ m s⁻¹. It is critical that all wet/dry checks be done at a small enough time interval so that the wetting/drying algorithm is not Courant surpassing. This latter condition artificially retards the wetting front as the surge progresses inland and the surge height will excessively build up behind the wetting front. Practically, this implies performing wet/dry checks at each model time step.

UnSWAN Model

SWAN (Simulating WAVes Nearshore) and UnSWAN are spectral wave models which predict the wave action density spectrum using the Action Balance Equation,

$$\frac{\partial N}{\partial t} + \nabla \bar{x} \cdot [(\bar{c}_g + \bar{U})N] + \frac{\partial c_\theta N}{\partial \theta} + \frac{\partial c_\sigma N}{\partial \sigma} = \frac{S_{tot}}{\sigma}$$

where:

$\frac{\partial N}{\partial t}$ = propagation of wave action in \vec{x} -space

\vec{c}_g = wave group velocity

\vec{U} = ambient current vector

N = wave action density

\vec{x} = geographic space

θ = wave direction

σ = relative frequency

c_θ = turning rate

c_σ = shifting rate

S_{tot} = wave growth by wind, action lost to whitecapping, surf breaking and bottom friction, and action exchanged between spectral components in deep and shallow water (Dietrich et al. 2011b).

Parameterizations of the above are given by Booij et al. (1999) and further modification, as of version 40.72, is given by Holthuijsen et al (2003) which includes the phase-decoupled refraction-diffraction. At present, diffraction has not been enabled (Dietrich et al. 2011b).

SWAN uses a triple loop to compute wave action densities. The innermost loop represents a sweep of the mesh in opposite directions to allow wave energy to propagate sufficiently throughout the domain. The next loop is a Gauss-Seidel iteration similar to that which is used within the structured version of SWAN. Finally, the outermost loop represents stepping through time.

Since SWAN is a spectral wave model, it does not attempt to resolve processes less than one wavelength, even in areas of very high resolution. This is a task more suited to a phase resolving wave model. This resolution, however, is not wasted as it is necessary to accurately solve complex topography.

b. Description of System being Represented by the Model

Storm surge and waves in southern Louisiana, are described by a coupled ADCIRC circulation, UnSWAN wave and PBL wind model system. The surge and waves propagate over an elevation surface that contains frictional parameterizations to reflect the real world system and physical interaction with fluids to correctly simulate inland flood propagation. Further details are described in Sections 1b and 1d.

c. Analytical Requirements

Not applicable.

d. Assumptions

Assumptions have been described in Section 1f. These assumptions are commonly made and applied for similar applications, such as the storm surge and wave analysis conducted as part of the LACPR study.

e. Identification of Formulas Used in the Model and Proof that the Computations are Appropriate and Done Correctly

See Section 2a.

3. System Quality**a. Description and rationale for selection of supporting Software Tool/Programming Language and Hardware Platform**

FORTRAN is the programming language used for UnSWAN. This is due to the 30-year history of the model.

The hardware platforms used to simulate the *OCPR20212* model are high-performance computing clusters. Parallel computing is commonly used for ADCIRC applications, as it's highly scalable. Details of the systems used are described in Section 3c.

b. Proof that the Programming was Done Correctly

Public release version of ADCIRC version 49 was applied. Validation results were as anticipated.

c. Availability of Software and Hardware Required by Model

ADCIRC and UnSWAN are both open-source, FORTRAN-based codes. The source code is available for download from <http://www.adcirc.org>. The programs both use the standardized MPI (Message Passing Interface) for parallel communications and have been tested with various MPI libraries and FORTRAN compilers.

Louisiana Optical Network Initiative, in conjunction with Louisiana State University, provided high performance computing resources for parallel computing. Queen Bee is a 50.7 TFlops Peak Performance, 668 compute node cluster running Red Hat Enterprise Linux version 4 operating system. Each node contains dual Quad Core Xeon 64-bit processors operating at a core frequency of 2.33 GHz.

In cooperation with the University of Notre Dame Center for Research Computing and Environmental Fluid Dynamics group, computer time was provided on the computing cluster Athos. Athos is an 83 node machine with 2 processors per node and 6 computational cores per processor, totaling 996 computational cores which communicate over an Infiniband system. The processors are based upon the Nehalem architecture which makes them much faster when compared to their predecessors at the same processor speed. This is due to their ability to use Intel's Quick Path Interconnect. This allows the computational cores on each processor to communicate directly with both memory and each other with no need for an intermediary. Communication between nodes is

handled by the Infiniband system which allows the nodes to communicate much faster than traditional methods. The computational cores operate at clock speed of 2.66 GHz, though true performance can be as much as twice that of other machines running older hardware.

d. Description of Process Used to Test and Validate Model

Hurricane Gustav was the first named storm to make landfall in Louisiana during the 2008 Atlantic hurricane season. Unlike previous storms, various agencies collected an unprecedented amount of time series and high water mark (HWM) data spanning the Louisiana coastline. FEMA provided measured high water marks, and time series data was provided by Andrew Kennedy (AK), the U.S. Army Corps of Engineers and Computational Hydraulics Lab (USACE-CHL), the U. S. Geological Survey (USGS) and the Coastwide Reference Monitoring System (CRMS).

The eye of the hurricane moved from southeast to northwest across the state. Gustav was significantly smaller and weaker than the last storm to make landfall in the southeast. Katrina, however, as it progressed, the radius affected by tropical storm strength or greater winds increased and the observed surge was larger than expected.

Hurricane Ike first made landfall in Cuba and tracked northwest across the Gulf eventually making its U.S. landfall near Galveston, Texas on September 13, 2008. At its maximum, Ike's tropical storm force and hurricane force winds extended out almost 275 miles and 90 miles respectively from its center generating significant wave heights up to 26 feet in the Gulf of Mexico. Ike's unprecedented size and track coupled with the distinctive bathymetry on the Texas shelf, created a forerunner surge that arrived almost 12 hours ahead of the storm (Kennedy, 2011). Sustained shore parallel currents caused a seven-foot water surface increase as the forerunner propagated along the Louisiana-Texas coast toward Galveston.

This combination of storms, Hurricane Gustav followed closely by Hurricane Ike, is a challenging exercise for determining model skill. Making landfall on opposite ends of Louisiana, the two storms collectively affected hundreds of miles of coastline. The quantity of data available for evaluating simulation results for these two storms is greater than available for any other storms to date along coastal Louisiana. Additionally, correctly hindcasting Hurricane Ike depends on correctly calculating the surge and waves from Hurricane Gustav since the storms occurred in such rapid succession. For these reasons, simulating the successive impact of these two storms was used to demonstrate the skill of the ADCIRC and SWAN models for this O CPR project. It should be noted that the ADCIRC model was not tuned to a particular storm. Rather the model relies on physics-based adjustments to work on a variety of storms over the entire Louisiana coastline.

Model Setup

The ADCIRC model was used to simulate water surface elevations and currents driven by winds, tides and fresh water inputs. Waves were simulated using the unstructured version of the UnSWAN model which is run at the same time as ADCIRC in a tightly coupled paradigm. ADCIRC was run with a one second time step and coupled to UnSWAN every 1,200 seconds during the simulation. The UnSWAN time step was set to 1,200 seconds to match the coupling interval. ADCIRC and UnSWAN are run on the same finite element mesh and ADCIRC shares its parameters such as Manning's n , directional wind reduction, wind and pressure forcing, water surface elevations and currents at each node throughout the domain with UnSWAN, which then passes wave radiation stress information

back to ADCIRC. These wave radiation stresses are then used until the next coupling interval occurs where new radiation stress information is received.

The mesh used for the validation exercise contains the fully open Inner Harbor Navigation Canal (IHNC) because construction of the Lake Borgne barrier was not complete when Hurricanes Gustav and Ike occurred. This allows for the exchange of water between Lake Pontchartrain and Lake Borgne via the IHNC. This area was taken directly from the SL16 ADCIRC mesh used to validate Hurricane Gustav in 2011 by Dietrich et al. Note that the production mesh used for evaluating future scenarios includes the closure of the Lake Borgne barrier.

As previously mentioned, Hurricanes Gustav and Ike occurred within a short time frame, so in order to accurately capture surge and currents in Ike, both hurricanes were run as a single simulation. This means that after Gustav was complete, the Ike simulation would begin with the waves, water surface elevations and velocities present at the end of the Gustav simulation. A schematic of the simulation timing is shown in Figure 155.

The simulation of Hurricane Gustav and Ike began at 0000 GMT on July 25, 2008. Tidal forcing and fresh water inputs in the Mississippi and Atchafalaya Rivers were applied at the model boundaries for 36 days until the hurricane winds were applied on August 30, 2008. Tidal constituents used during this time period were K1, K2, M2, N2, O1, Q1 and S2. Full descriptions of the tidal parameters can be found in Table 7.

Table 7 Tidal Constituents used for the Gustav/Ike simulation beginning on 7/25/2008 @ 0000GMT

Tidal Constituent	Amplitude	Frequency	Earth Tide Potential Reduction Factor	Nodal Factor	Equilibrium Argument (degrees)
K1	0.141565	0.0000729212	0.736	1.092	218.225
K2	0.030704	0.0001458423	0.693	1.244	256.990
M2	0.242334	0.0001405189	0.693	0.972	192.543
N2	0.046398	0.0001378797	0.693	0.972	236.809
O1	0.100514	0.0000675977	0.695	1.149	332.220
Q1	0.019256	0.0000649585	0.695	1.149	16.485
S2	0.112841	0.0001454441	0.693	1.000	0.000

Riverine inputs were also introduced at the Mississippi and Atchafalaya rivers using a river-wave radiation boundary which allow tides and surge to propagate past the boundary condition (Westerink et al. 2008, Bunya et al. 2010). During the aforementioned tidal component of the simulation, river influx is ramped up from zero to 8,920 cubic meters per second (m³/s) and 3,823 m³/s in the Mississippi and Atchafalaya rivers respectively, using a 5-day hyperbolic ramp function (Dietrich 2011). The extended ramp ensures the Atchafalaya basin fills completely during the 36 days of tidal forcing to set up an accurate condition once hurricane winds are applied. A current limitation of the ADCIRC model is the requirement that riverine inputs remain constant throughout the simulation. Hurricane Gustav river conditions were used throughout the entire simulation. Hurricane Ike saw a large increase in river flows in both the Mississippi and Atchafalaya River. Flow rates measured 12,225 m³/s and 5,239 m³/s in the two rivers, a 37 percent increase in flow from

what was measured during Gustav. Thus, it is expected that the gauge comparisons in both rivers should appear to have lower ADCIRC results than measured data during Hurricane Ike.

Tidal constituent parameters were calculated using the LeProvost Tidal Database. During the tidal forcing portion of the simulation, only ADCIRC was run. On August 30, the winds from Hurricane Gustav began and the UnSWAN model was coupled to ADCIRC. This portion of the simulation ran until September 2 and the model was allowed to again run with tidal forcing only. After the Gustav winds completed, the UnSWAN model was still active to allow waves to continue to propagate and set up an accurate initial condition for Hurricane Ike. Hurricane Ike forcing began on September 5, 2008 at 1200 UTC and lasted through September 14, 2008 at 0600 UTC. A 1.25 day period was incorporated to allow flow to continue to penetrate inland, as well as drain from the system after the storm.

Data assimilated wind forcing for both storms were provided by Oceanweather, Inc. The winds are provided as 30-minute sustained winds at 10 meters in height. These values are then interpolated to 15-minute intervals and multiplied by 1.09 to convert them to 10 minute sustained winds. (Bunya, 2010). A directional wind coefficient is applied to the winds, as previously described, to account for reduction in the winds by different landforms, such as trees, which reduce the wind forcing felt by the water column.

The ADCIRC model is constructed with bathymetry and topography relative to the North American Vertical Datum of 1988 (NAVD88). A value of 0.134m is added to the initial water surface to adjust the water surface to the NAVD88 datum (Garster et al. 2007, Bunya et al. 2010). The initial water surface is also adjusted to reflect thermal expansion and other seasonal effects in the Gulf of Mexico. The approximation for thermal expansion is computed using long term NOAA stations at Grand Isle, Eugene Island, and Dauphin Island. The computed adjustment is 0.119m. Finally, 0.025m is added to account for SLR between 2004 and 2008. The total initial water surface for the simulation of Hurricanes Gustav and Ike is $0.134 + 0.025 + 0.119 = 0.278\text{m}$ (ARCADIS 2001c).

The master plan validation model contained 1,148,270 nodes and 2,252,355 elements. This represents an 83 percent reduction in computational nodes from the mesh used by USACE (ARCADIS 2011c) (6,850,379 nodes) to validate Ike in the same single simulation paradigm. This reduction was necessary in order to produce a light weight model capable of analyzing many project scenarios for the Master Plan study.

2012 Coastal Master Plan Model Validation

Gustav

Figure 156 shows the maximum predicted water surface elevation during the simulation of Hurricane Gustav. As shown, this storm primarily exercises the eastern portion of the mesh leaving the westernmost third of the state largely unaffected by surge. Therefore, the majority of measured high water mark (HWM) and surge data is concentrated in the eastern portion of the state. Counter clockwise winds concentrate the highest surge in Lake Borgne and the Carnarvon Marsh. Maximum surge is almost 13 feet.

Figure 157 shows the differences between the measured high water marks and the computed high water marks from the ADCIRC and UnSWAN model run. Locations colored white in Figure 157 show high water mark locations that are within one foot of the measured values. Warm colors are where

ADCIRC over predicts by over a foot and cool colors are locations ADCIRC under predicts by over a foot. Much of the state falls within the +/- one foot difference range and almost entirely within the +/- two foot difference range. Figure 158 shows a correlation coefficient of 0.74 and slope of 0.98. Agreement is generally good throughout Barataria Bay and areas north. Predictions are slightly high interior to Lake Pontchartrain and south of Lake Maurepas. Moving west, Golden Meadow to Morgan City, the area where the eye tracked directly over, show excellent agreement in nearly all the high water marks measured.

Sample hydrograph comparisons for Gustav are shown in Figures 160 through 162 and their locations in Figure 159. Additional hydrograph comparisons for Hurricane Gustav can be found in Appendix D-24-E. ADCIRC output from the Hurricane Gustav simulation begins on August 30, 2008. Stations show generally skillful agreement with the measured tidal signal and peak surge.

USACE Station 01300, located in the Mississippi River south of New Orleans, shows that the river stages are correct and the tides and surge are correctly propagating up the river to the station. As previously mentioned, the ADCIRC model can only use a single river forcing during the course of a simulation at its current version (49.14). The forcing that was applied corresponded to Hurricane Gustav, and therefore we expect a match between measured and predicted water levels. Moving southwest to CRMS station 0374-H01 which lies just west of Terrebonne Bay near Dog Lake, the agreement continues to be excellent with the measured data. Tides match well and the correct draw down is calculated before the surge arrives. Surge leaves the area slightly more quickly than measured data shows, however this drop off corresponds directly with the end of the Gustav wind data (09/02/2008 @ 1200GMT) during the time between the two storms (Ike winds begin on 09/03/2008 @ 0000GMT) so it is possible that the problem is more related to the lack of wind data than to the ADCIRC model itself. CRMS station DCPBS03 is located just outside the Carnarvon marsh on the same latitude as Point a la Hache. This station shows a very strong correlation to the data in tidal signal, run up, peak surge, and drain off.

Ike

In contrast to Hurricane Gustav, Hurricane Ike affects a much larger region of the computational domain and is an excellent test for a very large portion of the model, with about 70 percent of the study area coast receiving six or more feet of surge and much of it receiving eight or more feet. Though the storm makes landfall in Galveston, Texas, the storm tracks in such a way that surge is forced into the Carnarvon Marsh and Lake Borgne as well as heavily inundating the Lake Calcasieu area all the way along the coast to the Atchafalaya Basin. Figure 163 shows the maximum predicted surge levels during Hurricane Ike followed by Figure 164 which shows the spatial distribution of high water mark measurements compared to ADCIRC predicted results. Locations colored white in Figure 164 show high water mark locations that are within one foot of the measured values. Warm colors are where ADCIRC over predicts by over a foot and cool colors are locations ADCIRC under predicts by over a foot. Like Gustav, almost all of the measured high water marks lie within the +/-2 foot difference bar shown in the correlation plot, Figure 165. The correlation (R^2) is 0.743 and slope shows slight under prediction at 0.957.

Hydrograph output was also recorded during Hurricane Ike. A full suite of hydrograph plots for Hurricane Ike can be found in Appendix D-24-F. Sample hydrographs are shown in Figures 167 through 169 and their locations in Figure 166. CRMS station 1069-H01 lies on the eastern side of the storm track just outside of Lake Borgne. Though not directly affected by Ike's eye, a surge of six and a half feet was pushed through the area by the passing storm. The hydrograph shows proper

phasing of the tidal signal as well as a nicely matching peak. As seen in the Gustav simulation, the drain off occurs more quickly than shown in measured data. However, the shape of the data is well captured. CRMS Station 0651-W01 is located between Lakes Calcasieu and Sabine in one of the hardest hit areas of Louisiana. Measured data shows a peak surge at this location of approximately eight and a half feet while ADCIRC over predicts slightly at nine feet. Finally, CRMS station 0345-H01 located on the west side of Terrebone Bay. This station shows agreement with tides and peak surge. However, the forerunner surge mentioned earlier, shown as the first large bump in the data on September 11 with an elevation of about three and a half feet, is under predicted by approximately three-quarters of a foot.

e. Discussion of the Ability to Import Data into Other Software Analysis Tools (interoperability issue)

Data is passed to other Master Plan models in an ASCII text based format that can easily be edited to any necessary format. For further details, see Section 1e.

4. Usability

a. Availability of Input Data Necessary to Support the Model

Data input required for the model is primarily elevation data for the mesh, land cover data for surface characteristic description and system forcing information (PBL wind and pressure fields for this study). Elevation and land cover data is readily available as part of the Master Plan effort. Additional elevation data from SL18 and land cover data from C-CAP is also readily available. PBL wind fields and all other forcing information carried forward from the LACPR study were provided in literature and from USACE.

b. Formatting of Output in an Understandable Manner

All output formats are described at <http://www.adcirc.org>. The user can choose between ASCII, binary, or NetCDF formats that can easily be edited to any other necessary format.

c. Usefulness of Results To Support Project Analysis

ADCIRC and UnSWAN can be used to provide impacts of proposed projects on storm surge, tides, nearshore waves and other hydrodynamic conditions for a variety of protection and restoration projects. The types of protection project that can be evaluated include structural flood protection (levees, floodwalls, and flood gates), and non-structural projects (relocations, elevation or flood-proofing of structures). Restoration projects that can be evaluated include barrier island restoration, marsh restoration, channel realignment and closures, coastal ridge restoration, freshwater and sediment diversions, and other types of restoration projects.

d. Ability to Export Results Into Project Reports

Several visual ADCIRC output products are available for use in project reports. Maps of the maximum surge elevation and maximum current velocity are available. Difference plots can also be made of those parameters, to evaluate differences between surge and wave values for various scenarios and project analyses. Time series output can also be extracted at point locations for inclusion in tables or hydrographs.

e. Training Availability

There are training options available. The ADCIRC Developers Group hosts an annual “ADCIRC Boot Camp” for those interested in learning the model.

f. Users Documentation Availability and whether it is User Friendly and Complete

The ADCIRC user manual is available at http://www.adcirc.org/document/ADCIRC_title_page.html.

g. Technical Support Availability

Technical support for SMS mesh generation software is provided by Aquaveo. Support for ADCIRC is provided by the user community via an email listserv, at <http://www.adcirc.org>.

h. Software/Hardware Platform Availability to All or Most Users

The software is free for download. Hardware can be desktop PCs. However, due to the solution size for this project, specialized high performance computers are necessary, which are usually housed at universities or government agencies. Usually, special arrangement must be made to have access to these high-performance computing resources.

i. Accessibility of the Model

The ADCIRC model is free to download and comes as a source code that is compiled by the end user. The `cmplrflags.mk` file that comes as part of the source code has many predefined compiler suites on various computing systems to serve as a template for other systems. ADCIRC uses the makefile system to build the various executables. The “make” command is standard on nearly all UNIX platforms. ADCIRC input files are set up according to the guidelines provided on <https://www.adcirc.org> input file descriptions page. These input files are the `fort.13`, `fort.14`, `fort.15`, `fort.22`, `fort.26` and `swaninit`. The end user can compile the code in serial or parallel. If a parallel code is preferred, the preprocessing code, ADCPREP, must be run first to set up the parallel run. The parallel version of the code is run using the commands specific to the MPI library installed on the particular machine.

j. Transparency of Model and how it Allows for Easy Verification of Calculations and Outputs

The ADCIRC theory and formulation report can be found on the ADCIRC website and are described in Section 2a. Calculations are verified during historic storm validation described in Section 3d.

The easiest means to verify outputs are the creation of images, which can be automated with ADCIRC output. Details for reviewing outputs using plots are described in Section 1e.

5. Sources of Model Uncertainty

The ADCIRC model solves the shallow water equations. As with any equation, they represent an approximation to reality. These equations and their derivations rely on certain assumptions which can present errors in themselves if they are not met. See Sections 2a and 2d for a discussion of

ADCIRC assumptions. Also, the code is run in its two-dimensional depth integrated form, which means three-dimensional currents are not resolved.

Error for both ADCIRC and UnSWAN arise from a poorly designed mesh. A mesh lacking the critical features and the mesh resolution to convey flow will not accurately reproduce measured data. Also, mesh topography and bathymetry must be an accurate representation the area which it attempts to replicate.

Finally, the ADCIRC and UnSWAN model is limited by its inputs. Between elevation sources, LULC data, meteorological forcing, and historical data for validation comparison, ADCIRC and UnSWAN rely heavily on inputs from other systems and surveys. ADCIRC and UnSWAN, like any other modeling system, operates under the assumption that the input data itself is correct.

6. Suggested Model Improvements

The ADCIRC and UnSWAN models themselves are not in need of any known fundamental improvements for capturing the dynamics of hurricane driven waves and storm surge. Through previous use in numerous other projects and through the validation performed specifically for this project, these models have demonstrated that they provide the desired level of accuracy and detail for surge and waves. Nonetheless, the ADCIRC model has been evolving for thirty years as computational methods become more efficient and physical systems better understood. This is a trend that is certain to continue. Ongoing ADCIRC research shows promising improvements for model computational speeds, with decreases in compute time by orders of magnitude. Improvements such as these allow for more highly resolved computational meshes and consequently create a need for improved tools to create, simulate and post process results.

The 2012 Coastal Master Plan models would have benefited from additional computational resources. If more and faster computer processors were available, the models could be run in less time which would allow for evaluation of more scenarios, a larger storm suit per scenario, and a shorter project schedule. Additional computer resources would also permit the resolution in the mesh to be increased which would in turn allow for inclusion of smaller scale features, such as narrow bayous that are not currently incorporated into the model.

While it is believed that the storm surge and wave components are being adequately served, the overall project could potentially benefit from a tighter coupling of a hydrodynamic model to the ecosystem components. The *OCPR2012* model has a very detailed representation of offshore bathymetry and on-land topography and roughness which could be used as the basis for a more comprehensive modeling system. For example, in addition to extreme events, the ADCIRC model can be used to simulate tidal and low-energy daily scenarios to explore changes in tidal prism and marsh hydroperiod for future scenarios. Spatially varying impacts to the tidal prism and marsh hydroperiod would better inform the wetland morphology and vegetation models of regional variance in future conditions. Additionally, a hydrodynamic model using the same finite element representation as *OCPR2012* could inform the distribution and time scales of transport for salinity, sediment, and nutrients, which could in turn enhance the understanding of subsidence, accretion, and changes in vegetation. Developing more comprehensive modeling paradigms would bring additional accuracy to the water quality and ecosystem models and would enhance the overall value

of the project. Finally, in a circuitous way, enhancing the eco-system dynamics will yield more accurate depictions of future land cover, marshes, and topography which would ultimately yield better surge estimates when those improved results are used to update the ADCIRC-UnSWAN model.

7. *Quality Review*

Specific QR procedures for the Storm Surge/Waves model to support the 2012 Coastal Master Plan included the following:

1. Review of the following outputs from the maximum value output dataset:
 - Maximum storm surge for seven zooms throughout Louisiana.
 - Maximum significant wave height for the seven zooms.
 - Peak wave period for the seven zooms.
 - Difference plots for maximum storm surge and significant wave height:
 - For the Year0+1Day simulations (S50_G90), the difference plots for surge were analyzed between 2007 LACPR output and Master Plan output.
 - For S12_G90, S11_G90 and S13_G90, the difference plots for surge and waves were analyzed between the given scenario and S50_G90.
 - G91-G97 storm suites were compared to the G90 storm suite for the same scenario.
2. Extraction of point location data for the Damage Assessment model following QR procedures for the maximum value output:
 - The only data posted to the CPRA FTP site were the point location data; thus a second round of QAQC procedures was incorporated to ensure that the point data are extracted and posted correctly.
 - Time series data for over 11,000 point locations were extracted for each storm. Because 40 storms were simulated for each suite, the team thinned the point location review set to approximately 100 points. Additionally, 10 of 40 storms were reviewed to ensure that a storm on each track was reviewed prior to posting the data.

8. *Uncertainty analysis*

ADCIRC and UnSWAN uncertainty is best quantified by comparing model output to measured data. Section 3d describes the model validation for Hurricane Gustav and Hurricane Ike. Figure 158 and Figure 165 show the comparison between model output and measured data for the two events. Comparison of ADCIRC model output to measured data was used as a guideline for sensitivity tests completed as part of the Risk Assessment Team uncertainty analysis.

9. References

- Arcement, G.J. and V.R. Schneider. 1989. "Guide for Selecting Manning's Roughness Coefficients for Natural Channels and Flood Plains", *U.S. Geological Survey Water-Supply Paper 2339*, U.S. Geological Survey, Denver, Colorado.
- ARCADIS. 2008a. "Investigation of ADCIRC Surge Results in St. Charles Parish." U.S. Army Corps of Engineers, New Orleans District. May 16.
- ARCADIS. 2008b. "Hydroperiod Modeling Study - Inner Harbor Navigation Canal Proposed Barrier Golden Triangle Marsh." May 23.
- ARCADIS. 2008c. "An Evaluation of Hurricane Storm Surge in the Mississippi River with High Stage Flows, Part I – Model Development and Validation." U.S. Army Corps of Engineers, New Orleans District. August 19.
- ARCADIS. 2008d. "Storm Surge Modeling Study - Inner Harbor Navigation Canal/Lake Borgne Proposed Barrier." U.S. Army Corps of Engineers, New Orleans District. December 22.
- ARCADIS. 2010. "An Evaluation of the Mississippi River Using the SL16 ADCIRC Mesh – Model Development and Validation." U.S. Army Corps of Engineers, New Orleans District. May 28.
- ARCADIS. 2011a. "Storm Surge and Wave Analysis of West Shore Lake Pontchartrain Hurricane Protection Projects." (Draft) U.S. Army Corps of Engineers, New Orleans District. April 22.
- ARCADIS. 2011b. "An Evaluation of the Atchafalaya River Using the SL17 ADCIRC Mesh." (Draft) U.S. Army Corps of Engineers, New Orleans District. May 23.
- ARCADIS. 2011c. "ADCIRC and STWAVE Hydraulic Modeling of Southwest Coastal Louisiana Hurricane Protection Projects." (Draft) U.S. Army Corps of Engineers, New Orleans District. May 26.
- ARCADIS. 2011d. "Storm Surge and Wave Modeling for the Master Plan Prioritization Tool - Phase 1: Preliminary Results and Model Selection Recommendations." Louisiana Office of Coastal Protection and Restoration. February 15.
- Atkinson, J.H., J.J. Westerink, and J.M. Hervouet. 2004. "Similarities between the Quasi-Bubble and the Generalized Wave Continuity Equation Solutions to the Shallow Water Equations," *International Journal for Numerical Methods in Fluids*, 45, 689-714.
- Barnes, H.H. 1967. "Roughness Characteristics of Natural Channels," *U.S. Geological Survey Water-Supply Paper 1849*, U.S. Geological Survey, Washington D.C.
- Booij, N., R.C. Ris, and L.H. Holthuijsen. 1999. "A Third-Generation Wave Model for Coastal Regions, Part I: Model Description and Validation," *J. Geophys. Res.*, 104(C4), 7649-7666.
- Bunya, S., and Coauthors, 2010: A high-resolution coupled riverine flow, tide, wind, wind wave, and storm surge model for southern Louisiana and Mississippi. Part I: Model development and validation. *Mon. Wea. Rev.*, 138, 345–377.

- Charnock, H. 1955. "Wind stress on a water surface." *Quart. J. Royal Met. Society*, 81: 639-640.
- Chow, V.T. 1959. "Open Channel Hydraulics," McGraw-Hill Book Company, New York.
- Dawson, C., J.J. Westerink, J.C. Feyen, and D. Pothina. 2006. "Continuous, Discontinuous and Coupled Discontinuous-Continuous Galerkin Finite Element Methods for the Shallow Water Equations," *Int. J. for Num. Meth. Fluids*, 52, 63-88.
- Dietrich, J.C., R.L. Kolar, and R.A. Luetlich. 2005. "Assessment of ADCIRC's Wetting and Drying Algorithm." School of Civil Engineering and Environmental Science, University of Oklahoma, Norman, Oklahoma, 73019. cdietrich@ou.edu.
- Dietrich, J.C., J.J. Westerink, A.B. Kennedy, J.M. Smith, R. Jensen, M. Zijlema, L.H. Holthuijsen, C. Dawson, R.A. Luetlich, Jr., M.D. Powell, V.J. Cardone, A.T. Cox, G.W. Stone, H. Pourtaheri, M.E. Hope, S. Tanaka, L.G. Westerink, H.J. Westerink, Z. Cobell. 2011a. "Hurricane Gustav (2008) Waves and Storm Surge: Hindcast, Synoptic Analysis and Validation in Southern Louisiana," *Monthly Weather Review*, 139, 2488–2522.
- Dietrich, J.C., M. Zijlema, J.J. Westerink, L.H. Holthuijsen, C. Dawson, R.A. Luetlich Jr., R.E. Jensen, J.M. Smith, G.S. Stelling, G.W. Stone. 2011b. "Modeling Hurricane Waves and Storm Surge Using Integrally-Coupled, scalable computations." *Coastal Engineering*, 58, 45–65.
- Federal Emergency Management Agency. 2005. "HAZUS: Hazard loss estimation methodology." <http://www.fema.gov/hazus/index.shtm>.
- Feyen, J.C., J.H. Atkinson, and J.J. Westerink. 2000. "Issues in hurricane surge computations using a GWCE-based finite element model." *Proc., XIII Conf. on Computational Methods in Water Resources*, Vol. II, L. Bentley, J. Sykes, C. Brebbia, W. Gray, and G. Pinder, Eds., 865-872.
- Galland, J., N. Goutal, and J. Hervouet. 1991. "A new numerical model for solving the shallow water equations." *Adv. Water Res.*, 14: 138-148.
- Garster, J., B. Bergen, and D. Zilkoski. 2007. "Performance Evaluation of the New Orleans and Southeast Louisiana Hurricane Protection System, Final Report of the Interagency Performance Evaluation Task Force, Volume II – Geodetic Vertical and Water Level Datums", U.S. Army Corps of Engineers, Washington, D.C. March 26.
- Henderson, F.M. 1966. "Open Channel Flow," Macmillan Publishing Company, New York.
- Holthuijsen, L.H., Herman, A., Booij, N., 2003. "Phase-decoupled refraction–diffraction for spectral wave models." *Coastal Engineering* 49, 291–305.
- Hsu, S. 1988. *Coastal Meteorology*. Academic Press, 260 pp.
- Kennedy, A.B., U. Gravois, B.C. Zachry, J.J. Westerink, M.E. Hope, J.C. Dietrich, M.D. Powell, A.T. Cox, R.A. Luetlich, R.G. Dean. 2011. Origin of the Hurricane Ike Forerunner Surge. *Geophysical Research Letters*, 38, In Press.

- Kubatko, E.J., J.J. Westerink, and C. Dawson. 2006a. "An Unstructured Grid Morphodynamic Model with a Discontinuous Galerkin Method for Bed Evolution," *Ocean Modeling*, 15, 71-89.
- Kubatko, E.J., J.J. Westerink, and C. Dawson. 2006b. "Discontinuous Galerkin Methods for Advection Dominated Problems in Shallow Water Flow," *Computer Methods in Applied Mechanics and Engineering*, 196, 437-451.
- Kubatko, E.J., J.J. Westerink, and C. Dawson. 2007. "Semi-discrete Discontinuous Galerkin Methods and Stage Exceeding Order Strong Stability Preserving Runge-Kutta Time Discretizations," *Journal of Computational Physics*, 222, 832-848.
- Kinmark, I. 1986. "The Shallow Water Wave Equations: Formulation, Analysis, and Application," *Lecture Notes in Engineering*, 15, Springer-Verlag, Berlin, 187 pp.
- Kolar, R.L., J.J. Westerink, M.E. Cantekin, and C.A. Blain. 1994. "Aspects of nonlinear simulations using shallow water models based on the wave continuity equation." *Comput. Fluids*, 23, 523-538.
- Kolar, R.L., and J.J. Westerink. 2000. "A Look Back at 20 Years of GWC-Based Shallow Water Models," *Computational Methods in Water Resources XIII*, Vol. 2, Bentley et al., eds. 899-906, Balkema.
- Le Provost, C., F. Lyard, J. Molines, M. Genco, and F. Rabilloud. 1998. "A hydrodynamic ocean tide model improved by assimilating a satellite altimeter-derived data set." *J. Geophys. Res. [Oceans]*, 103, 5513-5529.
- Louisiana State University. 2004. Louisiana Lidar. [Website] located at <http://atlas.lsu.edu/lidar/>.
- Luetlich, R.A., and J.J. Westerink. 1995. "Continental shelf scale convergence studies with a barotropic model." *Quantitative Skill Assessment for Coastal Ocean Models, Coastal and Estuarine Studies Series No. 47*, D.R. Lynch and A.M. Davies, Eds., Amer. Geophys. Union, 349-371.
- Luetlich, R.A., and J.J. Westerink. 1999. "Elemental wetting and drying in the ADCIRC hydrodynamic model: upgrades and documentation for ADCIRC version 34.XX." *Contractors Report*, U.S. Army Corps of Engineers. Available at: ERDC Vicksburg (WES), U.S. Army Engineer Waterways Experiment Station (WES), ATTN: ERDC-ITL-K, 3909 Halls Ferry Road, Vicksburg, Mississippi, 39180-6199.
- Luetlich, R.A., and J.J. Westerink. 2003. "Combined discharge and radiation boundary condition in the ADCIRC hydrodynamic model: theory and documentation." *Contractors' Report*, U.S. Army Corps of Engineers New Orleans District. Available at: U.S. Army Engineer Corps of Engineers, New Orleans, ATTN: CEMVN-IM-SM Library, P.O. Box 60267, New Orleans, Louisiana, 70160-0267.
- Luetlich, R.A., and J.J. Westerink. 2004. "Formulation and Numerical Implementation of the 2D/3D ADCIRC Finite Element Model Version 44.XX". [Website] located at http://adcirc.org/adcirc_theory_2004_12_08.pdf.
- Luetlich, R.A., J.J. Westerink, and N.W. Scheffner. 1992. "ADCIRC: an advanced three-dimensional circulation model for shelves, coasts and estuaries, report 1: theory and methodology of ADCIRC-2DDI and ADCIRC-3DL." Tech. Rep. DRP-92-6, U.S. Army Corps of Engineers. Available

at: ERDC Vicksburg (WES), U.S. Army Engineer Waterways Experiment Station (WES), ATTN: ERDC-ITL-K, 3909 Halls Ferry Road, Vicksburg, Mississippi, 39180-6199.

- Luettich, R.A. and J.J. Westerink. 2010. "ADCIRC User's Manual – v49." [Website] located at http://adcirc.org/documentv49/ADCIRC_title_page.html.
- Lynch, D.R., and W.G. Gray. 1979. "A wave equation model for finite element tidal computations." *Comput. Fluids*, 7, 207-228.
- Mukai, A., J.J. Westerink, R.A. Luettich, and D. Mark. 2002. "Eastcoast 2001: a tidal constituent database for the Western North Atlantic, Gulf of Mexico and Caribbean Sea," U.S. Army Corps of Engineers Research and Development Center, Coastal and Hydraulics Laboratory, Technical Report, ERDC/CHL TR-02-24. 201p. September.
- NOAA. 2007. "Sea level stations." [Website] located at <http://www.tidesandcurrents.noaa.gov/sltrends/sltrends.html>.
- NOAA. 2011. "Coastal Change Analysis Program." [Website] located at <http://www.csc.noaa.gov/digitalcoast/data/ccapregional/>.
- Powell, M., and S. Houston. 1996. "Hurricane Andrew's landfall in South Florida. Part II: Surface wind fields and potential real-time applications." *Wea. Forecasting*, 11, 329-349.
- Powell, M., S. Houston, and T. Reinhold. 1996. "Hurricane Andrew's landfall in South Florida. Part I: Standardizing measurements for documentation of surface windfields." *Wea. Forecasting*, 11, 304-328.
- Powell, M.D., P.J. Vickery, and T.A. Reinhold. 2003. "Reduced drag coefficient for high wind speeds in tropical cyclones." *Nature*, 422 (6929): 279-283 March 20, 2003.
- Reid, R.O. and R. Whitaker. 1976. "Wind-driven flow of water influenced by a canopy." *J. Waterw., Harbors, Coastal Engr. Div.- Am. Soc. Civ. Eng.*, 102, WW1, 61-77.
- Reid, R.O. 1990. "Water Level Changes - Tides and Storm Surges, Handbook of Coastal and Ocean Engineering," Gulf Publishing Co.
- Simiu, E., and R. Scanlan. 1986. "Wind Effects on Structures." *Wiley Interscience*, 604 pp.
- U.S. Army Corps of Engineers. 2008a. "Louisiana Coastal Protection and Restoration Technical Report." New Orleans District, Mississippi Valley Division. February.
- U.S. Army Corps of Engineers. 2008b. "Flood Insurance Study: Southeastern Parishes, Louisiana - Intermediate Submission 2." New Orleans District, Mississippi Valley Division. July
- U.S. Army Corps of Engineers. 2008c. "Flood Insurance Study: Southwestern Parishes, Louisiana - Intermediate Submission 2." New Orleans District, Mississippi Valley Division. October

Westerink, J.J. 1993. "Tidal prediction in the Gulf of Mexico/Galveston Bay using model ADCIRC-2DDI," Contractors Report to the U.S. Army Engineer Waterways Experiment Station, Vicksburg, Mississippi. January.

Westerink, J.J., and W.G. Gray. 1991. "Progress in Surface Water Modeling," Reviews of Geophysics, Supplement, 29, 210-217.

Westerink, J. J., and Coauthors, 2008: A basin- to channel-scale unstructured grid hurricane storm surge model applied to southern Louisiana. Mon. Wea. Rev., 136, 833–864.

DRAFT